applied sciences

MDPI

Article

Comparative Evaluation of Dichromate Adsorption Parameters Using Colorimetry on Glutaraldehyde-Crosslinked Polyethylene Imine (PEI) and Polyaniline (PANI)

Thomas Tunidau [1], Ashika Chandra [1], Taitusi Taufa [1], Ashneel Ajay Singh [1], Francis S. Mani [1], Xun Pan [2], Mats R. Andersson [2] and Desta Gedefaw [1,*]

[1] Discipline of Biological and Chemical Sciences, School of Agriculture, Geography, Environment, Ocean and Natural Sciences, The University of the South Pacific, Private Mail Bag, Suva, Fiji; thomas.tunidau@usp.ac.fj (T.T.); cao@polytech.ac.fj (A.C.); taitusi.taufa@usp.ac.fj (T.T.); ashneel.singh@usp.ac.fj (A.A.S.); francis.mani@usp.ac.fj (F.S.M.)

[2] Flinders Institute for Nanoscale Science and Technology, College of Science and Engineering, Flinders University, Sturt Road, Bedford Park, Adelaide, SA 5042, Australia; caroline.pan@flinders.edu.au (X.P.); mats.andersson@flinders.edu.au (M.R.A.)

* Correspondence: desta.gedefaw@usp.ac.fj

Abstract

Environmental pollution caused by hexavalent chromium [Cr(IV)] is a critical global concern due to its carcinogenic and acute toxicity. This study describes the synthesis of crosslinked polyethylene imine (PEI) and polyaniline (salt and base forms) and their effectiveness at removing dichromate ion ($Cr_2O_7^{2-}$) from aqueous solutions. The synthetized polymer adsorbents were comprehensively characterized using IR, TGA, and SEM-EDX methods. The adsorption processes were monitored via colorimetry and UV–Vis spectroscopy using the 1,5-diphenylcarbazide method under acidic conditions. Kinetic modeling revealed that the adsorption data fitted well to the pseudo-second-order model, confirming a chemisorption-controlled process. Equilibrium data followed the Langmuir isotherm at room temperature, predicting maximum adsorption capacities of 161 mg/g for PEI and exceeding 285 mg/g for the PANI salt. Thermodynamic parameters (ΔG°, ΔH°, and ΔS°) were all negative, confirming the spontaneous and exothermic nature of the adsorption process. In selective competitive studies, the PANI salt demonstrated exceptional robustness, maintaining a Cr(VI) removal efficiency of 93% to 99% in the concurrent presence of KH_2PO_4, $NaNO_3$, and $CuSO_4$ interferents, which is highly comparable to the control. Conversely, the removal efficiency of PEI was sensitive to the matrix, dropping to 52–53% in the presence of $NaNO_3$ and $CuSO_4$ while remaining unaffected (65%) by KH_2PO_4. Furthermore, regeneration studies using 5% HNO_3 demonstrated stable reusability, with both polymers maintaining high adsorption efficiencies (88–99%) over four consecutive cycles. These findings highlight the significant potential of these accessible polymeric materials for functional integration into real-world industrial wastewater treatment facilities.

Keywords: hexavalent chromium; crosslinked polyethylene imine; polyaniline salt; colorimetry; adsorption kinetics; adsorption isotherms; coexisting ions

Academic Editor: Antony C. Calokerinos

Received: 28 August 2026
Revised: 20 October 2026
Accepted: 23 October 2026
Published: 3 November 2026

Copyright: © 2026 by the authors. Licensee MDPI, Basel, Switzerland. This article is an open access article distributed under the terms and conditions of the Creative Commons Attribution (CC BY) license.

1. Introduction

Environmental contamination by heavy metals and other pollutants is a serious health concern [1–3]. Chromium is a heavy metal and a significant environmental pollutant due to its extensive use in various industrial applications, including manufacturing pigments and dyes, leather tanning, metal corrosion inhibition, catalysts, surface coatings, and wood and water treatment [4–6]. Chromium occurs in various oxidation states ranging from +2 to +6 but is most frequently found in the environment in the trivalent (Cr^{3+}) and hexavalent (Cr^{6+}) oxidation states, with Cr^{6+} accounting about 10% to 15% of total chromium usage for various applications [7]. Cr^{3+} has lower toxicity and mobility in the environment than Cr^{6+}, which is a known human carcinogen [8], and has high mobility, posing significant environmental and health risks. Cr^{6+} is a potent oxidizing agent that poses significant health risks upon entering the body, particularly affecting the lungs, liver, brain, and kidneys [9,10]. In fact, the toxicity of Cr^{6+} has been reported to be 500 times more than that of Cr^{3+} [5,11]. Due to its high toxicity and carcinogenic potential, Cr^{6+} levels in the environment are strictly regulated to protect human health and ecosystems. To mitigate the health risks associated with chromium exposure, regulatory guidelines mandate low levels of chromium, generally below 0.1 ppm (100 ppb) for total chromium in drinking water, with the WHO specifically recommending levels below 0.05 ppm (50 ppb) [12].

To maintain the level of heavy metals including chromium at a safe level and, hence, reduce health crisis, several treatment techniques have been developed, which include flocculation, membrane filtration, chemical precipitation, ion exchange, and adsorption precipitation methods. Adsorption techniques of heavy metals using adsorbents have been widely researched. For instance, the use of activated carbon as an adsorbent to treat wastewater and remove pollutants is well documented. McKay et al. used activated carbon to remove Cr^{3+} from water and reported a removal efficiency of 35 mg/g [13]. Biochar (a carbonaceous material obtained from different biomass by heating to high temperatures in a limited oxygen environment) is another adsorbent material heavily studied and used to treat water. Biochar prepared from coconut shells, for example, was reported to have a Cr^{6+} adsorption efficiency of 4.72 mg/g at 25 mg/L [14,15]. Biochar created from invasive plants as feedstocks has also been reported in the past with the intention of preparing a high-value material. Biochar produced from water hyacinth, for example, showed a copper adsorption efficiency of 28.2 mg/g. Synthetic and biopolymers are among the materials used as alternative adsorbent material for water treatment [16]. For instance, poly(butyl methacrylate) (PBMA) modified with resorcinarenes was used recently to remove dichromate from water and was reported to have a maximum adsorption efficiency of 81.1% at pH 5.0 in 1 h [17]. The use of crosslinked polyethylene imine (PEI), polyaniline, and composites at removing heavy metals and capturing CO_2 and other toxic organic and inorganic pollutants has been investigated, and success stories from researchers across the globe have been reported [18].

PEI is a water-soluble and nitrogen-rich synthetic polymer that exists either in linear and branched forms (Figure 1) [19]. However, by introducing small organic crosslinkers such as glutaraldehyde, the stability of PEI is enhanced, making the resulting material insoluble in water (Scheme 1) and mechanically strong [20–23]. A recent study highlighted the potential of crosslinked PEI, showing a significant copper adsorption efficiency of 253 mg/g from 0.075 mol/L copper solution [24]. A conducting carbon cloth coated with crosslinked PEI film has also been used to adsorb copper ions from water and subsequently release them via electrochemistry, regenerating the adsorbent film for multiple uses [24,25]. The porous coating was found to store and release ~72 μgcm^{-2} of Cu^{2+} over multiple cycles by passing a 1 $mAcm^{-2}$ current density through the electrode in

artificial seawater [25]. PEI-functionalized poly(vinyl alcohol) microspheres were used to remove Cr^{6+} from water and reported a maximum removal capacity of 396.83 mg/g [26].

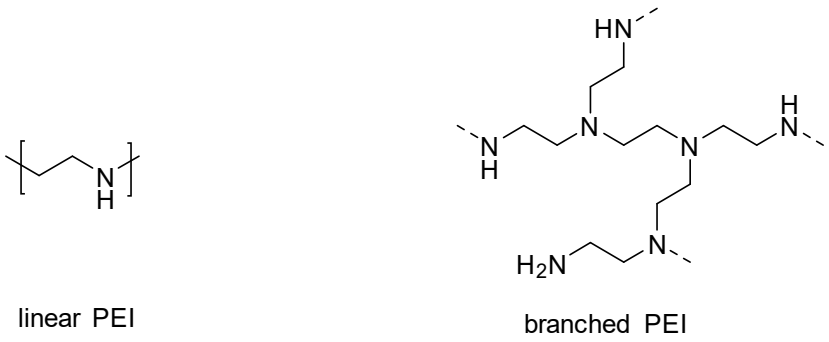
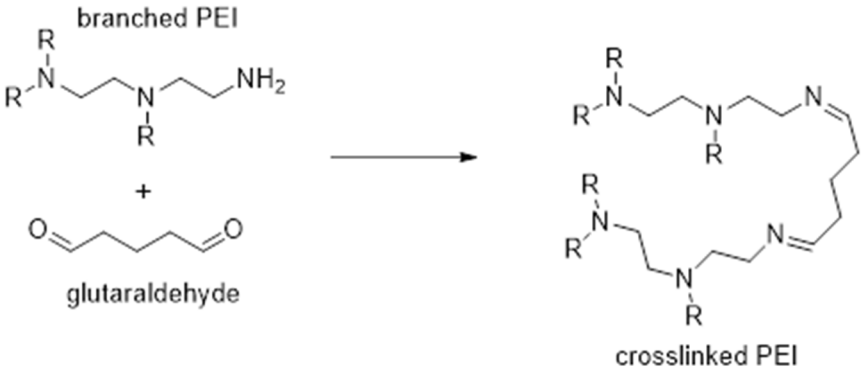


Figure 1. Types of PEI architectures.



Scheme 1. Proposed crosslinking reaction of PEI with glutaraldehyde by Schiff base formation [19].

On the other hand, polyaniline (PANI) is a versatile polymer with diverse applications in various fields, including anticorrosion coatings, batteries, sensors, and others. PANI is an inexpensive polymer with high environmental stability. It can be synthesized via the oxidative chemical polymerization of aniline using ammonium persulfate, ferric chloride, and potassium permanganate [27] and electrochemically in acidic media [28,29]. PANI exists in three main forms—leucoemeraldine, pernigraniline, and emeraldine—which are differentiated by the oxidation level of the polymer backbone [30]. Figure 2 illustrates the salt and neutral/base forms of emeraldine, which can interconvert simply by controlling the pH of the solution [31,32].

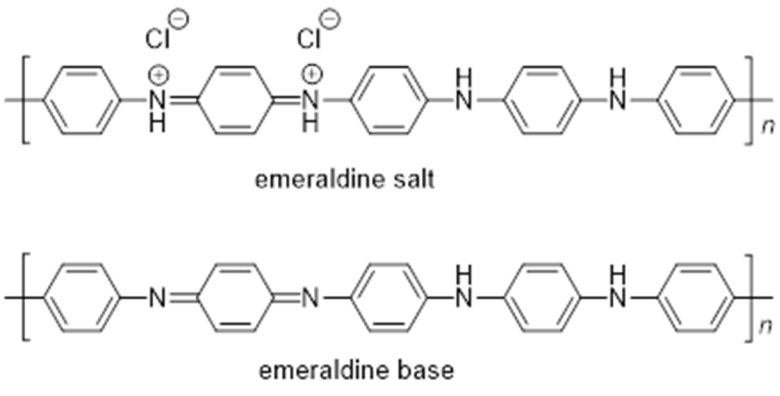


Figure 2. Chemical structure of PANI salt and base prepared by oxidative polymerization of aniline using ammonium persulfate as an oxidizing agent [31,32].

The presence of the benzene ring and charged nitrogen in the backbone of the PANI salt chain allows the polymer to have a favorable electrostatic interaction with charged pollutants. Hence, this property makes PANI and its composite materials highly effective for various environmental remediation applications such as removing heavy metals and dyes from contaminated water. In a study by Duhan et al., PANI nanofibers were prepared by interfacial polymerization, where the aniline monomer was dissolved in toluene while placing the oxidizing agent (ammonium sulfate) and HCl in a water phase, allowing the polymerization reaction to occur at the interface between the two phases. The base form of PANI was obtained by washing with 1 mol/L ammonia, and the resulting material was used to successfully removed methylene blue (cationic dye) from water solutions with 91% efficiency [27]. PANI and its composites have also been utilized to remove several heavy-metal pollutants from the environment [33]. A composite composed of magnetite/graphene/PANI (Fe_3O_4/G/PANI) demonstrated a high efficacy in removing Cr^{6+} ions, achieving an 86% removal efficiency within 20 min [34]. In another study, polyaniline–cobalt composite nanorods were synthesized, capable of removing Pb^{2+} with 99.6% efficiency [35]. These findings highlight the significant potential of PANI-based composites in treating heavy-metal contamination.

Despite these promising individual advancements in polymer-based remediation, a critical gap remains in the systematic, head-to-head comparative evaluation of PEI and PANI (in both salt and neutral/base forms) under identical experimental conditions. Most of the existing literature focuses on complex, multi-component nanostructured composites such as magnetite–graphene or metal-oxide hybrids, which significantly increase synthesis costs, processing times, and scalability barriers for real-world water treatment facilities. Furthermore, the explicit competitive adsorption behavior and selectivity profiles of these fundamental polymeric matrices in multi-ionic water systems containing co-existing salts (such as KH_2PO_4, $NaNO_3$, and $CuSO_4$) have not been fully elucidated.

To address these limitations, this study explicitly establishes the direct dichromate ($Cr_2O_7^{2-}$) adsorption capacity, kinetics, isotherms, and thermodynamic properties of easily accessible, non-composite crosslinked PEI and PANI matrices. Utilizing a synchronized analytical framework combining colorimetry [24,34,35], UV–Visible spectroscopy, Infrared Spectroscopy, Scanning Electron Microscopy paired with Energy-Dispersive X-ray Spectroscopy, and thermogravimetry, we map the material properties and their dichromate adsorption behaviors. Crucially, this work provides a robust matrix-interference profiling analysis on the dichromate adsorption capacity of the two polymers. The study also demonstrated a comprehensive four-cycle desorption validation using 5% HNO_3. By shifting the focus back to accessible, easily regenerated bulk polymers, this paper delivers a practical, cost-effective blueprint for scaling up efficient hexavalent chromium remediation workflows in industrial wastewater treatment. To the best of our knowledge, this is the first study to report the use of crosslinked PEI powder, synthesized with an HPMC additive for the removal of dichromate from water. The adsorption characteristics of the two adsorbents were evaluated under identical experimental conditions, giving highly representative adsorption data. A simple, cost-effective colorimetric technique coupled with UV–Visible spectroscopy was mainly used to assess the adsorption characteristics of the two adsorbents. We have also used AAS to evaluate the adsorption and desorption efficiencies.

2. Materials and Methods

2.1. Hazard Classification of the Major Chemicals

The chemicals used in this study were obtained from commercial sources and used as received. The hazard classification and safety precautions can be found in the Aldrich

Catalogue (https://www.sigmaaldrich.com). The chemicals used in this study are toxic if swallowed, inhaled, or when in contact with the body, and some of the chemicals are toxic to aquatic life with long-lasting effects; hence, necessary precautions should be taken.

2.2. Synthesis of PANI Salt and PANI Base

In a 100 mL beaker, 7.5 g of ammonium persulfate was dissolved in 75 mL of 1 mol/L HCl solution. In another 100 mL beaker, 2.50 g of aniline was dissolved in 75 mL of 1 mol/L HCl, and the solution was stirred for 30 min. The ammonium persulfate/HCl solution was added slowly to the aniline/HCl monomer solution over 10 min, and the mixture was stirred for 60 min. The solid formed was collected by suction filtration. The solid was washed with 1 mol/L HCl solution, distilled water, and acetone to remove unreacted monomer, excess initiator, and oligomers. The solid PANI salt (green in color) was further suspended in 250 mL of DI water and stirred overnight, and the solid was collected by filtration and dried in an oven at 80 °C for 6 h [31].

A total of 1.85 g of the green PANI salt was mixed with 25 mL of 0.2 mol/L NaOH and stirred at room temperature. The color of the mixture turned blue immediately. The solid was collected by suction filtration after 30 min stirring, washed with distilled water repeatedly, and then washed with acetone and dried at 65 °C for 30 min to yield a blue solid (PANI base).

2.3. Synthesis of Crosslinked PEI

In a beaker, 2.0 g of PEI (50 wt. %) and hydroxypropyl methylcellulose (HPMC) (0.2 g) were combined with 20 mL each of distilled water and acetonitrile, and the resulting mixture was stirred for 10 min. Glutaraldehyde (1.5 mL) (50 wt.%) was added to the mixture and stirred with a magnetic stirrer. The solid formed was collected by filtration after 24 h of stirring. The solid was then transferred into another beaker and stirred in distilled water for 24 h. The solid was collected by filtration and dried in an oven at 60 °C overnight, yielding dried polymer powder [19].

2.4. IR Study on Polymers

Fourier Transformation Infrared Spectroscopy (FTIR) (PerkinElmer Spectrum 100 Instrument, Serial Number 76563, equipped with a universal ATR, PerkinElmer Inc., Shelton, CT, USA) was used to record the absorption spectra of the crosslinked polymers. Typically, polymers (2–3 mg) were placed into the FTIR spectrometer, and a force garage of 70 was applied. The scanning of the polymers was carried out in the range of 450 cm^{-1} to 4000 cm^{-1}.

2.5. SEM and EDX Analysis

SEM was performed using an FEI Inspect F50 Field Emission scanning electron microscope (FEI Company, Eindhoven, The Netherlands) [36] at an accelerating voltage of 5 kV. The EDX analysis was carried out using a scanning electron microscope equipped with an Amatek EDAX EDS detector (EDAX Inc. (AMETEK Materials Analysis Division), Mahwah, NJ, USA). All samples were prepared by spraying the powder on double-sided conductive carbon tape, followed by sputter coating 5 nm of Pt.

2.6. Dichromate Solution Preparation, Treatment of Dichromate Solutions with Polymers, and UV–Visible Spectroscopy Analysis

A series of dichromate standard solutions were prepared by diluting three stock solutions (10, 100, and 1000 ppm) with distilled water. The 2, 4, 6, 8, and 10 ppm standard solutions were generated from a 10 ppm stock solution. Similarly, 30, 40, 50, 100, 200, and 250 ppm dichromate were prepared from the 100 and 1000 ppm stock solutions. Then, 10

mL of the 10, 30, 50, 100, 200, and 250 ppm dichromate solutions were transferred into a centrifuge tube with 0.015 g of PEI, and the 100, 200, and 250 ppm samples were treated with 0.015 g of PANI salt and placed on a shaker for 1 h (SF1 Stuart flask shaker) at an oscillation speed of 600 OSC/min. The liquid phase was passed through a 0.45 µm syringe filter and collected in a vial. The standards (2–10 ppm) and the filtrate of the treated polymers (2 mL) (100, 200, and 250 ppm PEI-treated aliquots were further diluted at 1:35 ratio) and were added into a separate glass vial. To each vial, 1 mL of 0.2 mol/L H_2SO_4, followed by 1 mL of 1,5-diphenylcarbazide solution (0.5% *w*/*v* in acetone), was added and gently mixed. The UV–Visible absorption spectrum of the solutions were recorded after 5 min of mixing [37].

2.7. Adsorption Kinetics Study of PEI and PANI Salt

Five centrifuge tubes were prepared, each containing 0.015 g of PEI and 10 mL of 300 ppm dichromate solution. The centrifuge tubes were sealed and placed on a shaker. The first tube was removed from the shaker after 0.5 h, followed by the other tubes after 1, 3, 5, and 24 h (PEI) and 1, 2, 6, and 24 h (PANI salt) of shaking. Aliquots from each tube were filtered using a 0.45 µm syringe filter. Filtered aliquots from PEI were further diluted at a 1:35 ratio, and then 2 mL of the diluted solution was mixed with 1 mL of 0.2 mol/L H_2SO_4 and 1 mL of 1,5-diphenylcarbazide (0.5% *w*/*v* in acetone). The resulting violet-colored solutions were analyzed using a UV–Visible spectrometer. This exact procedure was also used to measure the adsorption kinetics of the PANI salt samples but without dilution of the filtered dichromate solutions.

2.8. Adsorption Isotherms and Thermodynamic Properties of the Adsorption

To 10 mL of dichromate of different concentrations (250, 300, 350, and 400 ppm), 0.015 g of PEI was added and placed on a shaker for 24 h. In the same way, 10 mL of dichromate (at concentrations of 250, 300, 350, and 400 ppm) was treated with PANI salt and agitated for 24 h. Filtered aliquots from PEI-treated samples were further diluted at a 1:35 ratio. Then, 2 mL of both the diluted (PEI) and undiluted filtrate (PANI salt) were mixed with 1 mL of 0.2 mol/L H_2SO_4 and 1 mL of 1,5-diphenylcarbazide (0.5% *w*/*v* in acetone) and then analyzed with a UV–Visible spectrometer. The experiments were conducted at 28 °C and 38 °C.

2.9. Desorption of Dichromate from the Dichromate-Loaded Polymers and AAS Analysis

Dichromate (10 mL, 100 ppm) was adsorbed on 0.065 g of PEI and PANI following a similar procedure to that described above. Then, the solids were collected by gravity filtration and washed with DDW several times. The solids were dried at room temperature overnight. The solids were transferred to a centrifuge tube, and 1 mol/L of HCl (10 mL) and 1 mol/L of NaOH (10 mL) were added and agitated on a shaker for 4 h. The liquid part was then collected by filtration and diluted before it was analyzed using AAS (Perkin Elmer Atomic Absorption Spectrophotometer PinAacle 500, PerkinElmer Inc., Singapore). Standard solutions (2–10 ppm) of dichromate solutions were analyzed with AAS. A total of 0.0174 g of PEI and 0.0425 g PANI salt were added to 300 ppm and 600 ppm dichromate solutions and shaken for 24 h. The solid were collected and treated with 5% HNO_3. The recyclability of the materials was monitored using UV–Vis spectroscopy. The adsorption–desorption cycles were also investigated using a 600 ppm initial dichromate concentration (10 mL) with 0.04 g of PANI salt and PEI. A total of 20 mL of 5% HNO_3 was used as an eluent for the dichromate, and the recyclability was assessed via AAS.

3. Results and Discussion

The synthesis of PANI and crosslinking reaction of PEI are both simple, room-temperature reactions that can be conducted using basic laboratory glassware (beaker/flask). Figure S1, Supporting Information, illustrates the morphology and color of glutaraldehyde-crosslinked PEI, PANI salt, and PANI base. The crosslinked PEI is distinctly orange in color. The PANI emeraldine salt, initially a green color powder synthesized under acidic conditions, converts to the emeraldine base upon neutralization with 0.2 mol/L NaOH, a transformation evidenced by the visual color change from green to blue (Figure S1, Supporting Information).

The synthesized polymers displayed low solubility in various organic solvents. Both the PANI salt and the glutaraldehyde-crosslinked PEI were found to be insoluble in acetic acid, chloroform, and pyridine. On the other hand, the PANI base was sparingly soluble in both chloroform and pyridine, forming characteristic blue solutions. The higher solubility in pyridine resulted in a visibly darker blue solution when compared to the color intensity achieved in chloroform. However, the addition of acetic acid to the PANI base causes it to precipitate and become insoluble due to the formation of the PANI acetate salt. For applications requiring PANI adsorbent films or composite materials, the PANI base can be dissolved in pyridine and cast using techniques like blade coating [38]. Subsequent acidic treatment converts the material to the PANI salt form, thereby optimizing the material for specific applications. PANI films can also be deposited on conducting substrates, such as indium tin oxide (ITO), by using electrochemical methods [39]. In contrast, the preparation of crosslinked PEI films utilizes a two-step procedure: initially, the non-crosslinked PEI is deposited onto a substrate (e.g., carbon cloth) via spray coating, and then the film is crosslinked using crosslinking reagents (e.g., glutaraldehyde) [25].

Figure 3 shows the IR spectra of the three polymers (PEI, PANI salt, and PANI base). The crosslinked PEI spectrum features a prominent, broad N–H stretching peak between 3250 and 3650 cm^{-1}, whose breadth is attributed to hydrogen bonding in the material. This peak is weak in the spectrum of the PANI base and completely absent in the spectrum of the PANI salt. Two strong absorption peaks at 2927 cm^{-1} and 2829 cm^{-1} were observed in crosslinked PEI, characteristic of the C–H stretching vibrations of its methylene (CH_2) group. The presence of a peak at 1650 cm^{-1}, corresponding to the C=N bond, confirms the formation of the Schiff base from crosslinking of PEI with glutaraldehyde. Strong to medium peaks were observed at 1590, 1495, 1300, 1050, 985, and ~850 cm^{-1}. The peaks at 1590 cm^{-1} and 1495 cm^{-1} were attributed to the C=C stretching modes of the quinoid and benzenoid rings unique to the two PANI forms [40]. A weak-to-average peak at 1300 cm^{-1} indicates that the C–N bond is common in all three polymers. Furthermore, the strong peak at ~1050 cm^{-1} and moderate peaks at 985 cm^{-1} and 850 cm^{-1} in the PANI base and salt can be ascribed to C–H deformation vibrations of the benzene ring [41].

Scanning Electron Microscopy (SEM) and Energy-Dispersive X-ray Spectroscopy (EDX) were employed to characterize the surface morphology and elemental composition of crosslinked PEI and PANI salt samples, and the results are illustrated in Figures 4 and 5, respectively. SEM images show that the crosslinked PEI surface consists of irregularly shaped lumps and spherical particles. The material also showed micro-porosity, which likely formed from the leaching of some of the hydroxypropyl methylcellulose (HPMC) component during the water treatment, as HPMC is sparingly soluble in water and has a tendency of washing out from the blend when soaked in water. This increased porosity is expected to enhance the adsorption capacity of the material by providing more accessible sites for analytes.

EDX analysis of the crosslinked PEI revealed atomic percentages of 73.86% carbon, 19.63% nitrogen, and 5.83% oxygen (Table 1 and Figure 4). While the pure PEI polymer is

expected to have a theoretical 2:1 carbon-to-nitrogen ratio, the crosslinked PEI exhibited a higher ratio of ~4:1. This carbon enrichment is attributed to the integration of the crosslinker (glutaraldehyde) and the presence of residual, carbon-rich HPMC. Furthermore, the 5.83% oxygen content further confirms that HPMC remains in the structure. While HPMC was added to facilitate the formation of a porous adsorbent, its detection suggests that the current leaching process is incomplete. To fully remove the sparingly soluble HPMC and create the intended voids, the material should be soaked in water for a longer duration (more than 24 h) to achieve maximum porosity. The Pt detected is due to the coating of Pt on the material surface to allow for the conductivity required by SEM.

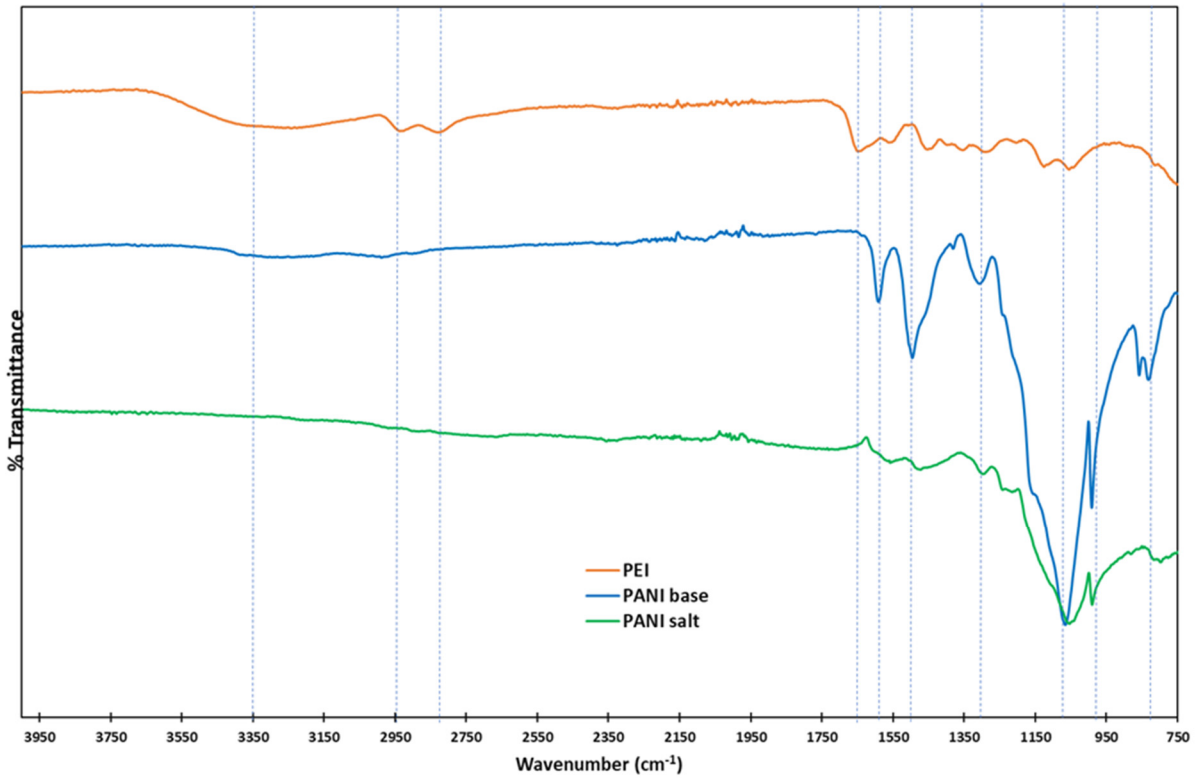
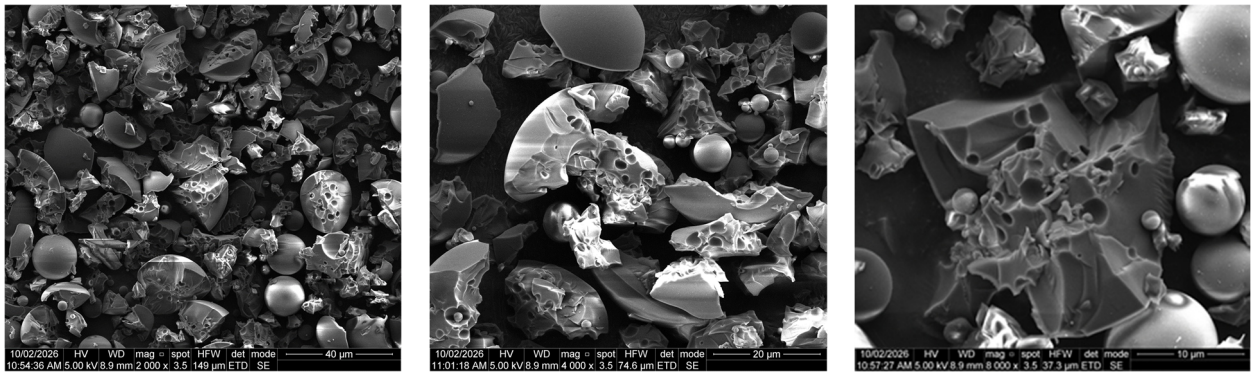


Figure 3. IR spectra of PEI, PANI base, and PANI salt.



https://doi.org/10.3390/app162110916

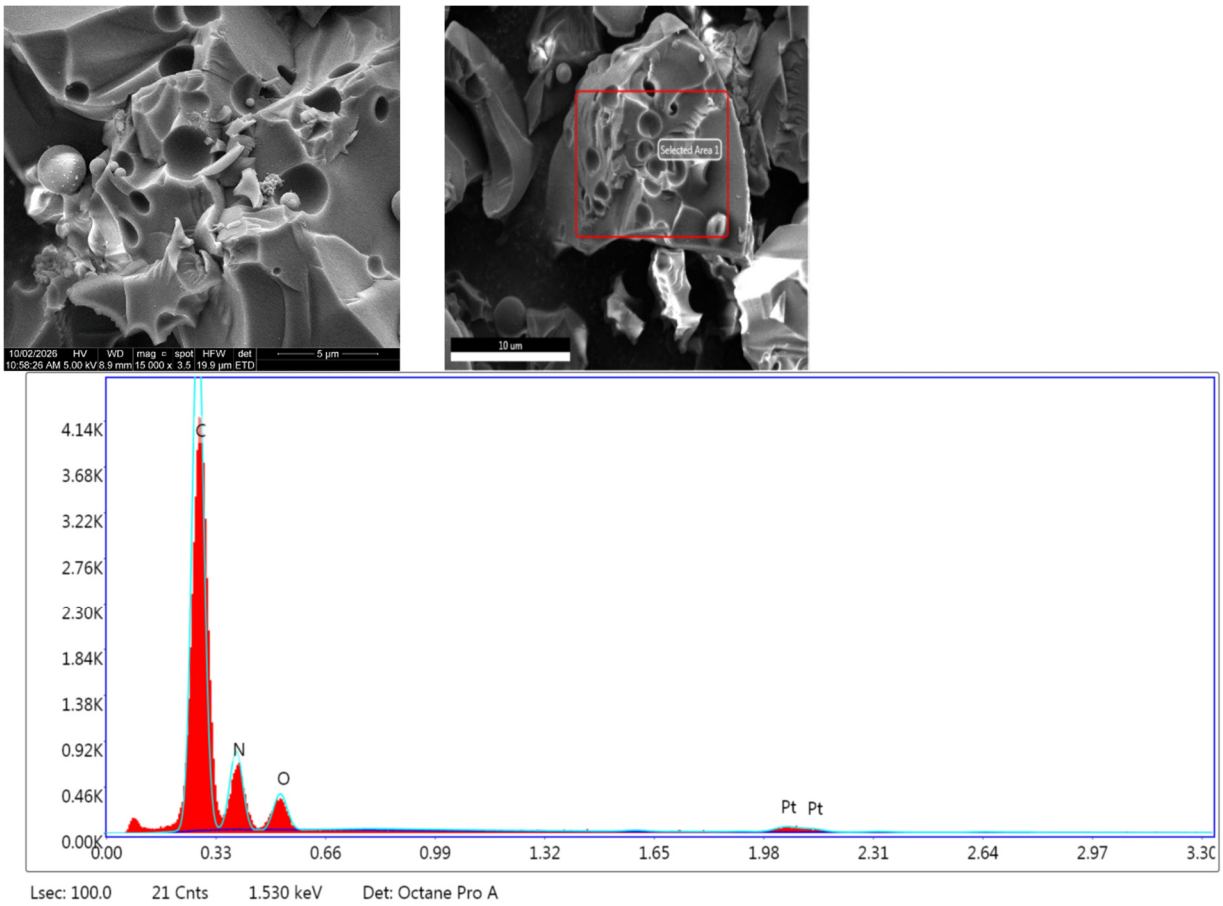
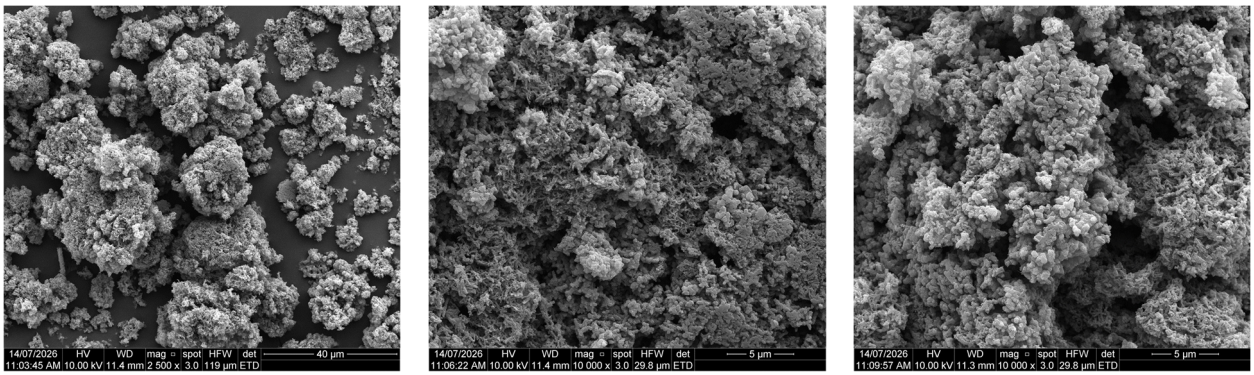


Figure 4. SEM images and EDX atomic percentage profile of PEI.

Similarly, Figure 5 presents the SEM micrographs of the PANI salt at varying magnifications. These images reveal the morphological features across both micro- and nano-scales, providing insight into the adsorbent's surface and the internal structure (up to 5 µm into the sample/support) of the adsorbent material. In the micrographs of PANI salt, compact structures are not formed. Instead, a mix of interconnected rod-like and spherical network develops, giving a porous nature of the adsorbent. This type of morphology increases the surface area of the material for a suitable interaction with the analyte to occur.



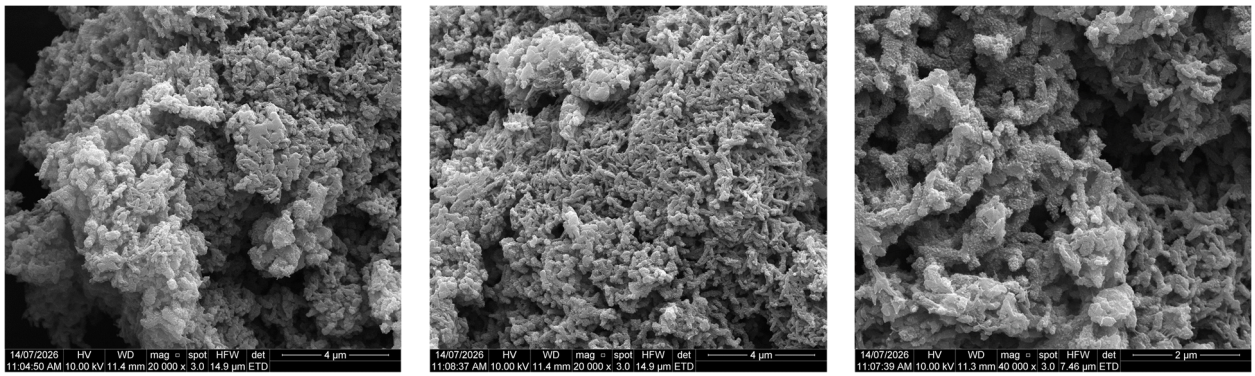
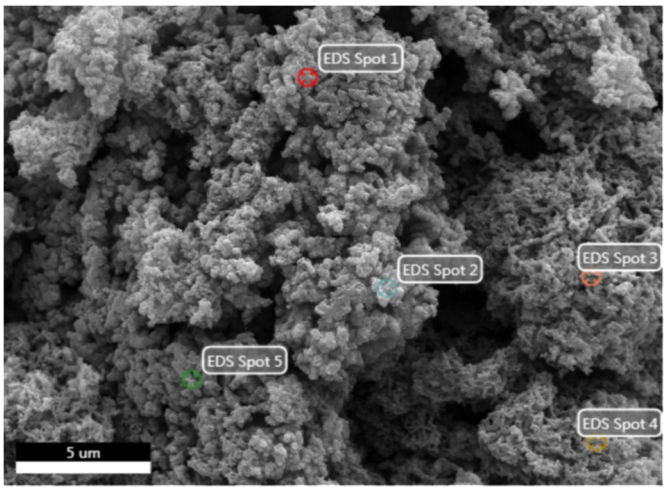
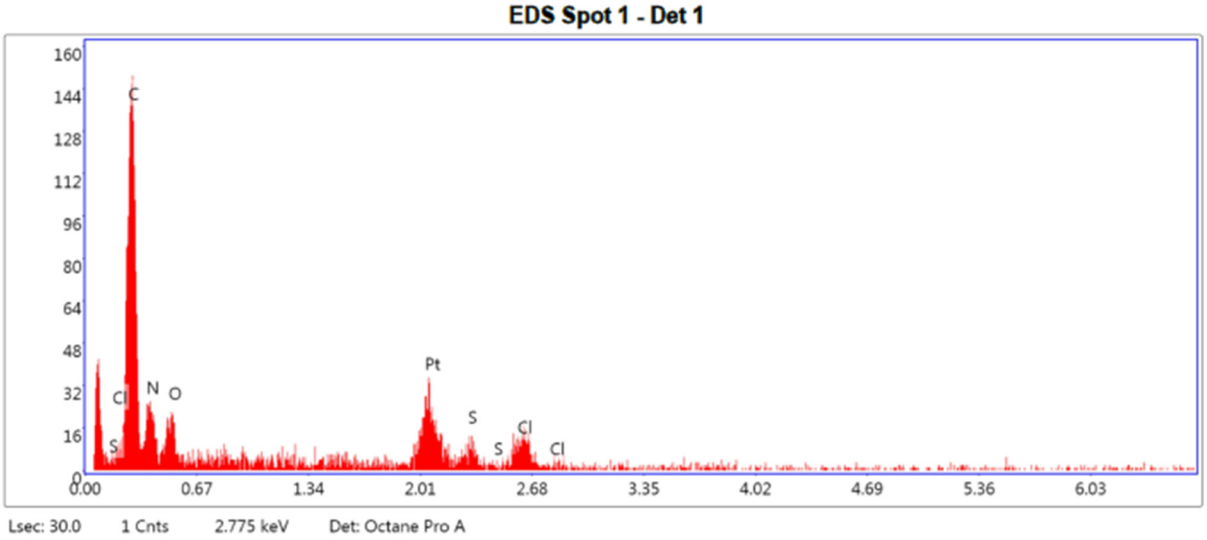


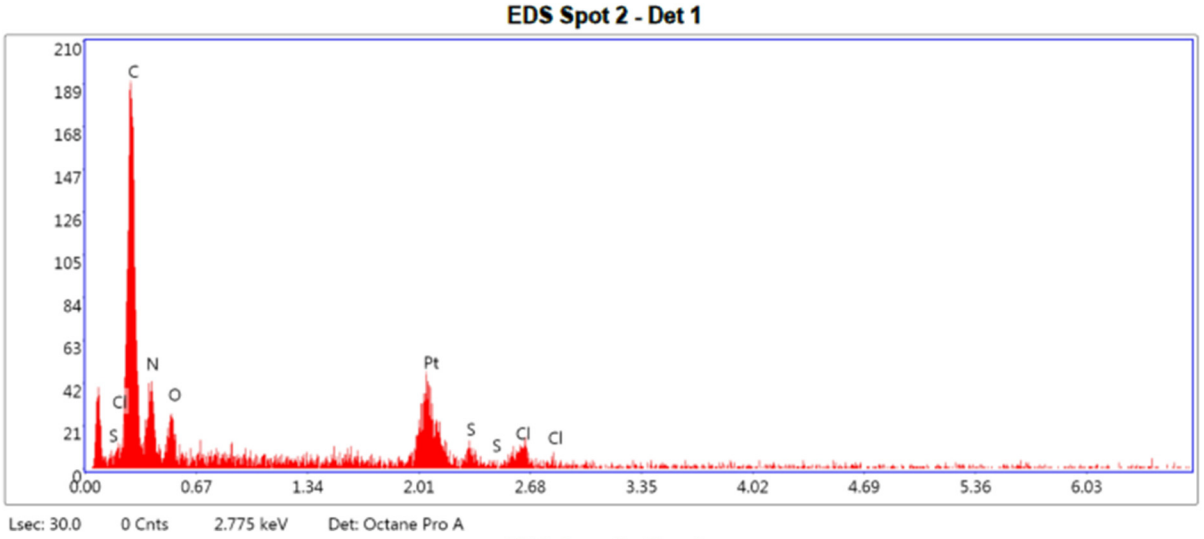
Figure 5. SEM images of PANI salt at varying magnifications.

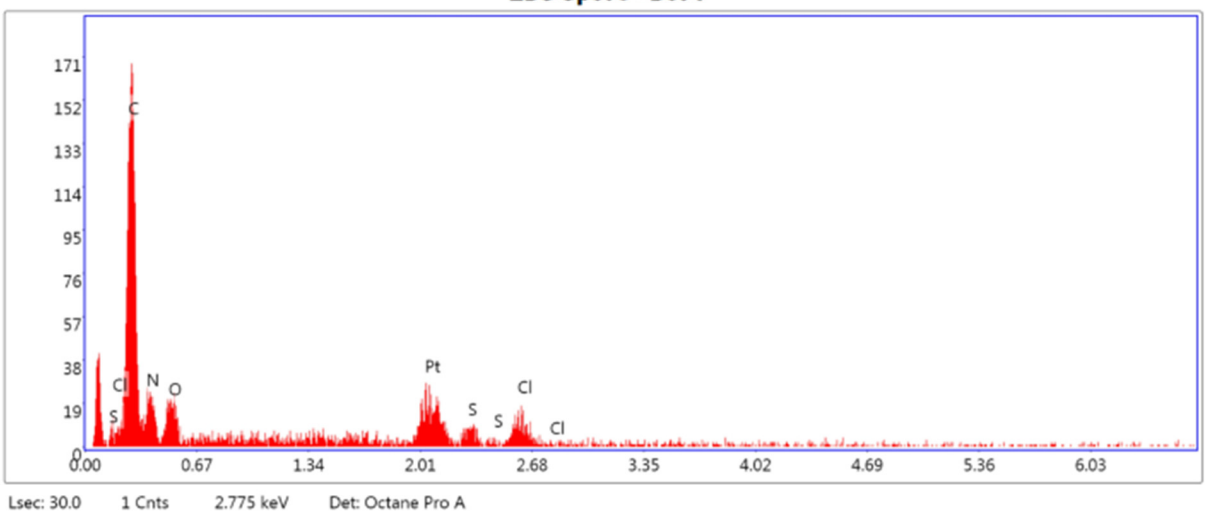
To ascertain the elemental composition of the PANI salt adsorbent material, EDX analysis was carried out on various sites. The results for five specific regions (identified as spots 1–5 in Figure 6) are summarized in Table 1. The corresponding EDX spectra for PANI salt are also given in Figure 6. Analysis revealed a nearly identical elemental distribution across the samples, consistent with polyaniline's structure. The elemental composition displayed is 69.72–74.31% carbon, 13.73–20.27% nitrogen, 5.05–6.8% oxygen, 0–0.87% sulfur, 2.64–7.9% chlorine, and 0.98–4.54% platinum. The detection of oxygen and sulfur may be attributed to residual ammonium persulfate used as an oxidizing agent in the polymer synthesis. The presence of chlorine is expected, as it originates from the HCl medium used during the oxidative polymerization reaction.

The EDX spectra of five regions on the PANI sample are shown in Figure 6.









https://doi.org/10.3390/app162110916

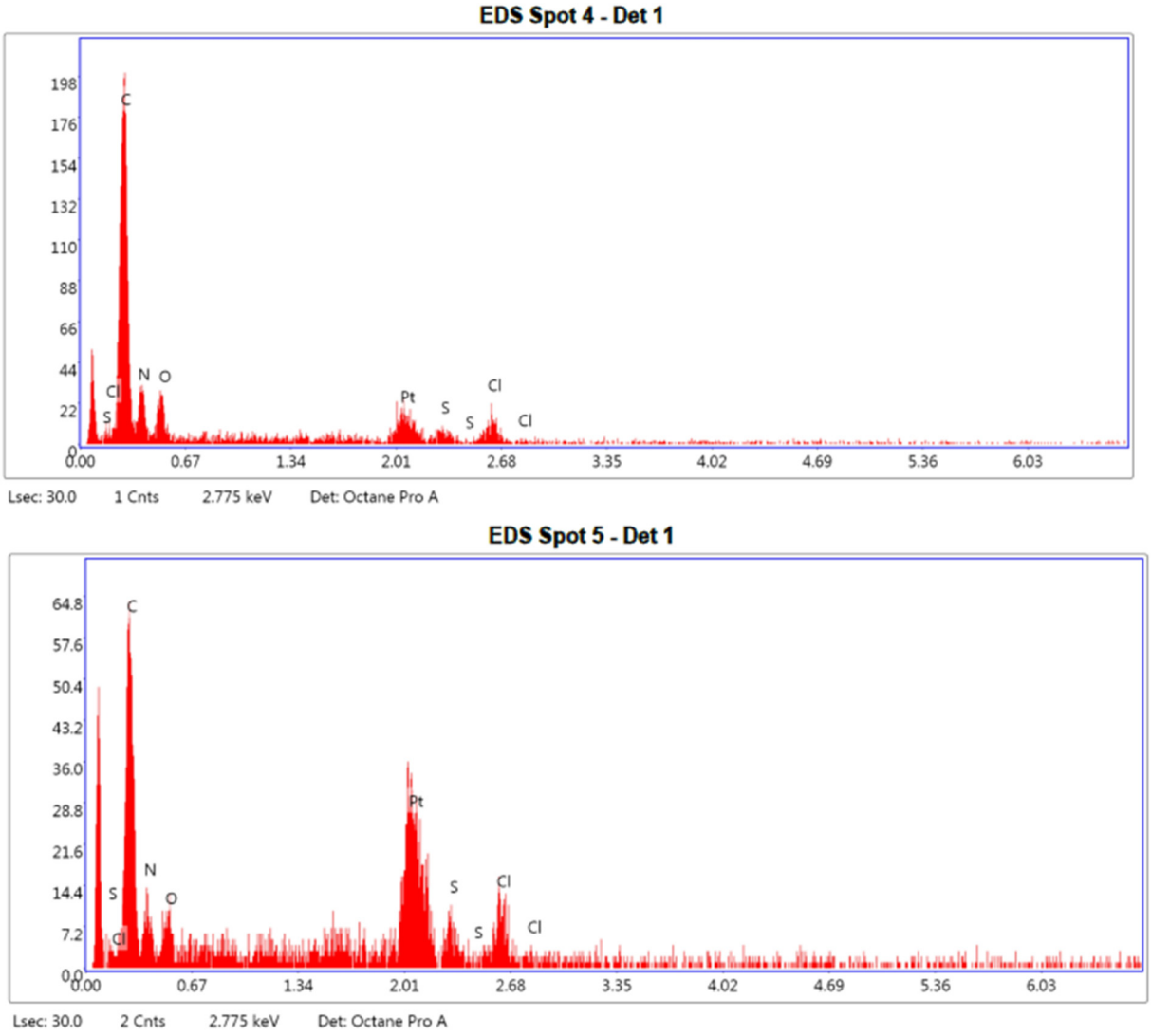


Figure 6. EDX spectra generated from 5 regions on the PANI salt sample.

3.1. Effect of Initial Concentration of Dichromate and Adsorbent Dosage on Adsorption Efficiency

The dichromate adsorption efficiency of the three polymers was quantified using UV–Visible spectroscopy via the 1,5-diphenylcarbazide colorimetric method. Standard solutions with concentrations ranging from 2 ppm to 10 ppm were prepared. For each analysis, 2 mL of each of the standard solution was mixed with 1 mL of 0.2 mol/L H_2SO_4 and 1 mL of 1.5-diphenylcarbazide (0.5% *w*/*v* in acetone). After gentle mixing and allowing the solutions to stand for 5 min, the mixtures developed a distinct pink coloration. The intensity of this color varied proportionally with the original dichromate concentration, facilitating quantitative analysis via UV–Visible spectroscopy (Figure 7) [26,37]. Details of the solution preparation for the UV–Visible measurement are as follows: The numbers written on the vials in Figure 7 represent the concentration of the dichromate used to prepare the solutions. For example, number 2 refers to the pink solution obtained from mixing 2 mL of 2 ppm dichromate standard solution with 1 mL of 0.2 mol/L H_2SO_4 and 1 mL of 1,5-diphenylcarbazide (0.5% *w*/*v* in acetone).

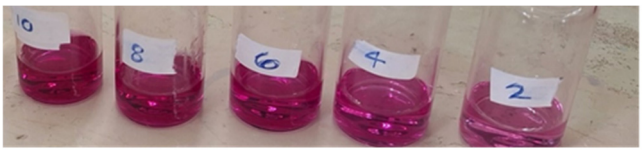


Figure 7. A mixture of 2 mL of each of the standard dichromate solutions (2, 4, 6, 8, and 10 ppm), 1 mL of H_2SO_4 (0.2 mol/L), and 1 mL of 0.5% *w*/*v* 1,5-diphenyl carbazide in acetone.

The UV–Visible absorption spectra of the standard solutions were analyzed (Figure S2, Supporting Information), revealing a peak absorbance at 542 nm. A standard calibration curve was plotted using the absorbance at this wavelength against the calculated dichromate concentrations in the 4 mL pink-colored mixtures. This provided a perfect linear equation ($y = 0.3883x + 0.04$) (Figure S2, Supporting Information).

A total of 10 mL of 10 ppm dichromate solution was placed into three centrifuge tubes, where each tube was then treated with 0.015 g of PEI, PANI salt, or PANI base, respectively, and left on a shaker at 600 OSC/min for 1 h. The solutions treated with PEI and PANI salt became colorless, indicating the quantitative removal of the dichromate ions. In contrast, the PANI base-treated solution resulted in a strong pink color, similar to the untreated 10 ppm dichromate solution. The UV–Visible absorption spectrum of the PANI base-treated sample showed an almost identical maximum absorbance as the control, implying that the dichromate ions were not adsorbed by the PANI base (Figure 8d). Due to the high adsorption efficiency displayed by both PEI and PANI salt at this low dichromate concentration (10 ppm), further tests were conducted using higher concentrations (30, 50, 100, 200, and 250 ppm for PEI (Figure 8a,b) and 100, 200, and 250 ppm for PANI salt (Figure 8c)). This was done to establish a correlation between the initial dichromate concentration and adsorption efficiency of the two polymers.

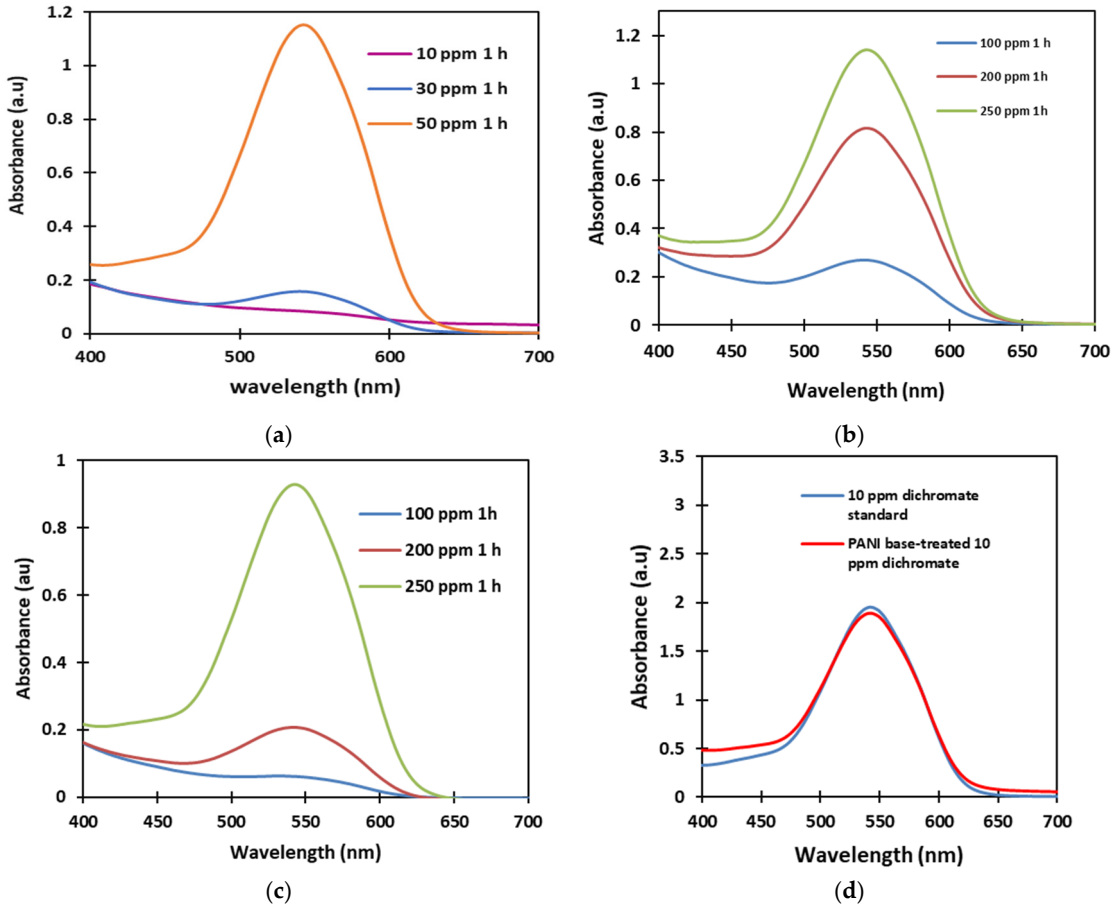


Figure 8. UV–Visible absorption spectrum of 10 mL dichromate treated with 0.015 g of adsorbents for 1 h: 10, 30, and 50 ppm dichromate solution treated with PEI (**a**); 100, 200, and 250 ppm dichromate solutions treated with PEI for 1 h (diluted 35 times) (**b**); 100, 200, and 250 ppm dichromate solutions treated with PANI salt (**c**); 10 ppm dichromate standard and PANI base-treated dichromate solution (**d**).

The dichromate removal efficiencies of the three polymers—PEI, PANI salt, and PANI base (all at 0.015 g per 10 mL of solution)—were calculated after 1 h treatment, and the values are summarized in Table 2. The adsorption efficiency of 0.015 g of PEI with 10 mL of 30 ppm and 50 ppm dichromate was also measured. PEI was found to be highly effective, capable of removing 98.000% of the dichromate ion from both 10 ppm and 30 ppm solutions within 1 h of agitation at 600 OSC/min. However, when the concentration of the dichromate increased to 100 ppm, 200 ppm, and 250 ppm, the removal efficiency of PEI dropped slightly to 58.368%, 30.050%, and 20.543%, respectively. In contrast, the dichromate removal efficiency of PANI salt was tested using a higher concentration (100, 200, and 250 ppm), which resulted in a removal percentage of 99.900%, 99.550%, and 98.160% for the 100, 200, and 250 ppm samples, respectively. As expected, PANI salt removed dichromate quantitatively at lower concentrations (10, 30, and 50 ppm). Therefore, the performance of PANI salt was higher than that of PEI, which could probably be attributed to the different adsorption mechanism of the PANI salt, which might dominantly involve electrostatic interaction with the salt form of the reactive nitrogen sites, compared to that of PEI. Interestingly, a similar study using the neutral base form of PANI revealed minimal dichromate adsorption. This indicates that the mechanism for dichromate removal of PANI salt relies on an ion exchange or cation–anion electrostatic interaction, which is absent or minimal with the base-washed polyaniline.

The effect of the adsorbent dosage on the dichromate adsorption efficiency was also briefly examined. Three centrifuge tubes containing 10 mL of 600 ppm dichromate solutions were treated with 0.015 g, 0.025 g, and 0.035 g of PANI salt and shaken for 24 h. Similarly, 10 mL of the same dichromate solution was added to three centrifuge tubes containing 0.015 g, 0.025 g, and 0.035 g of PEI and shaken for 24 h. The % dichromate removal efficiency is shown in Figure 9. It is evident that the dichromate removal efficiency improves with an increase in the adsorbent dosage. Specifically, 0.025 g and 0.035 g of PANI salt showed a quantitative removal efficiency of 99.050% and 99.72%. In contrast to this, 0.015 g of PANI salt removed 83.781% of the dichromate. Similarly, the dichromate removal efficiency of 0.015 g, 0.025 g, and 0.035 g of PEI was measured to give 30.908%, 41.807%, and 46.509%, respectively. In this case also, an increase in the PEI loading improves the dichromate removal efficiency but was found to be lower compared to that of the PANI salt.

Table 1. Summary of the elemental composition of PEI and PANI salt (spots 1–5).

PEI			PANI Salt									
			Element	Spot 1		Spot 2		Spot 3		Spot 4		Spot 5	
Element	Weight %	Atomic %		Weight %	Atomic %	Weight %	Atomic %	Weight %	Atomic %	Weight %	Atomic %	Weight %	Atomic %
C	63.86	73.86	C	53.94	73.98	48.93	69.72	57.33	74.31	57.97	72.50	40.08	71.95
N	19.79	19.63	N	13.03	15.32	16.59	20.27	13.30	14.78	15.97	17.13	8.92	13.73
O	6.71	5.83	O	4.91	5.05	4.80	5.13	6.43	6.26	7.24	6.80	5.05	6.80
Pt	9.65	0.69	Pt	19.75	1.67	24.05	2.11	15.29	1.22	12.72	0.98	41.11	4.54
			S	1.69	0.87	1.04	0.55	1.64	0.80	-	-	0.37	0.25
			Cl	6.69	3.11	4.59	2.22	6.02	2.64	6.09	2.58	4.48	2.73

Table 2. Adsorption efficiency of PEI (from 10 mL of 10 ppm, 30 ppm, and 50 ppm, 100 ppm, 200 ppm, and 250 ppm dichromate), PANI salt (from 10 mL of 100 ppm, 200 ppm, and 250 ppm dichromate), and PANI base (10 ppm dichromate) with 1 h of shaking at 600 OSC/min (adsorbent mass is 0.015 g).

Polymer	Concentration of Dichromate Ion (ppm)		Mass of Dichromate Ion (mg)		Adsorption Efficiency	
	Before Adsorption	After Adsorption	Not Adsorbed	Adsorbed	mg/g	%
PEI	10	0.113	0.002	0.098	6.533	98.000
	30	0.606	0.006	0.294	19.600	98.000
	50	5.729	0.057	0.443	29.533	88.600
	100	41.632	0.416	0.584	38.912	58.368
	200	139.900	1.399	0.601	40.067	30.050
	250	198.644	1.986	0.514	34.238	20.543
PANI salt	100	0.106	0.001	0.999	66.596	99.900
	200	0.862	0.009	1.991	132.758	99.550
	250	4.583	0.046	2.454	163.600	98.160
PANI base	10	9.532	0.095	0.005	0.468	5.000

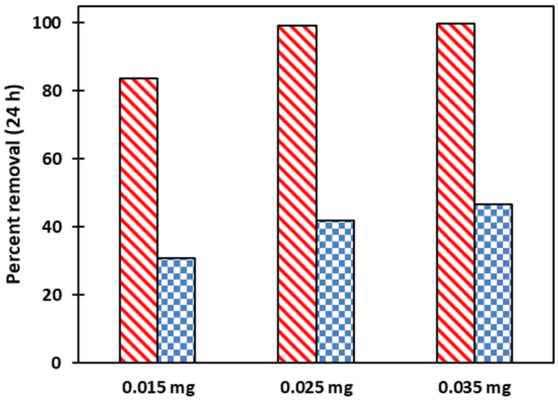


Figure 9. Effect of PANI salt dosage (**stripes**) and PEI dosage (**dotted**) from 600 ppm dichromate.

3.2. Adsorption Kinetics

The adsorption kinetics of PEI and PANI salt were assessed, with both having a remarkably high adsorption efficiency for dichromate. Briefly, 10 centrifuge tubes were used in this experiment. First, 0.015 g PEI was added to the first five tubes, and 300 ppm dichromate solutions were added. Similarly, 0.015 g of PANI salt was added to the other five tubes, and 10 mL of 300 ppm dichromate solutions were added to each tube. The tubes were placed on a shaker. Two tubes from each category were stopped after 0.5 h. The other tubes were removed from the shaker after 1, 3, 5, and 24 h (PEI) and 1, 2, 6, and 24 h (PANI salt) of shaking. Following filtration, the PEI-treated aliquots were further diluted at a 1:35 ratio, whereas the PANI salt-treated aliquots were analyzed without further dilution. A 2 mL volume of each sample was then reacted with 1 mL of 0.2 mol/L H_2SO_4 and 1 mL of 0.5% *w*/*v* 1,5-diphenyl carbazide in acetone. The resulting UV–Visible absorption spectra were recorded, and the corresponding profiles are presented in Figure S3, Supporting Information.

As expected, the decrease in absorption intensity over time indicates the continuous and increasing adsorption of the dichromate ions by the adsorbing materials.

The amount of dichromate adsorbed per gram of adsorbent (PANI salt and PEI) was calculated at various time intervals and is plotted in Figure 10. The data clearly illustrate that the adsorption process is rapid during the initial 5 h, after which the rate of adsorption slows down. Remarkably high removal efficiencies were observed for both materials. After 5 h of shaking, the removal efficiency reached 62% for PEI and 98% for the PANI salt when treated with an initial 300 ppm dichromate solution. After 24 h, the adsorption efficiency of the PANI salt further improved to 99%, whereas that of PEI plateaued at ~62%. This stagnation indicates that the active adsorption sites of PEI saturate early in the process, contrasting with the progressive uptake demonstrated by the PANI salt. The results represent a nearly quantitative removal of dichromate from the solutions with PANI salt while PEI showed a moderate adsorption efficiency. The adsorption capacities after 24 h were determined to be 125 mg/g for PEI and 199 mg/g for PANI salt from 300 ppm dichromate solution. However, it should be noted that the actual adsorption capacities could increase further with higher initial dichromate concentrations, as demonstrated by the equilibrium adsorption isotherm study presented later in this work. The isothermal study conducted by varying the concentration of the initial dichromate concentration from 250 to 400 ppm provided the maximum dichromate adsorption capacity of the two materials, reaching up to 161 mg/g for PEI, with a higher capacity of up to 285 mg/g for PANI salt (linear Langmuir model). Fitting the experimental adsorption data to various kinetic models is a standard procedure used to analyze adsorption kinetics. This process helps determine the underlying adsorption mechanism,

analyze the kinetics, and find additional useful parameters that enhance the overall understanding of the adsorption process.

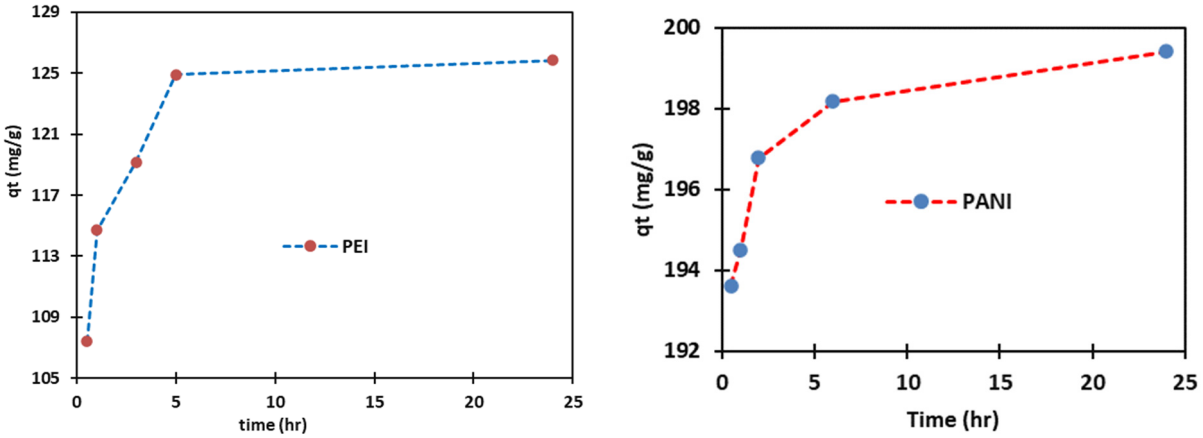


Figure 10. Adsorption amount (mg/g) of 0.015 g of the polymers with 10 mL of dichromate: 300 ppm (PEI) and 300 ppm (PANI salt).

In this study, the experimental data obtained from 10 mL of dichromate treated with 300 ppm (PEI/PANI salt) were specifically modeled using three commonly applied kinetic models: Elovich (Equation (1)), [42] pseudo-second-order (Equation (2)) [43], and pseudo-first-order kinetic models (Equation (3)).

$$q_t = \frac{1}{\beta}\ln(\alpha\beta) + \frac{1}{\beta}\ln(t) \quad (1)$$

The Elovich kinetic model is described by Equation (1), where qt represents the amount of adsorption (mg/g) at any time t, while α and β refer to the initial adsorption rate in mg/(g.min) and Elovich constant (g/mg), respectively. The Elovich model, widely used to study the adsorption behavior of gases onto heterogeneous surfaces and solids, is now frequently applied in the study of pollutant removal processes. This model operates under the fundamental assumptions that a chemisorption interaction occurs between the analyte and the adsorbent [44,45].

$$\frac{t}{q_t} = \frac{1}{K_2\, qe^2} + \frac{t}{q_e} \quad (2)$$

In the pseudo-second-order equation (Equation (2)), qe and qt represent the adsorbed analyte at equilibrium and at any time, t, respectively, and K_2 is the rate constant for the adsorption kinetics [46].

$$\log(q_e - q_t) = log q_e - \left(\frac{K_1}{2.303}\right) t \quad (3)$$

In the pseudo-first-order equation, qe and qt, respectively, refer to the amounts of adsorbate per unit weight of adsorbent (mg/g) at equilibrium and any time t, while k_1 (min^{-1}) represents the rate constant for pseudo-first order model.

The results from linear kinetic modeling are presented in Figure 11, which shows the graphs of the three kinetic models. Table 3 (linear and nonlinear pseudo second order) and Table 4 (pseudo first order and Elovich) provides a summary of the numerical values and parameters derived from these linear and nonlinear kinetic models.

Table 3. Summary of adsorption parameters of the linear pseudo-second-order and nonlinear pseudo-second-order models (fitting was carried out using Excel Solver).

Polymer	Linear Pseudo Second Order			Nonlinear Pseudo Second Order			
	K_2 (g/(mg.min))	q_e (mg/g)	R^2	K_2 (g/(mg.min))	q_e (mg/g)	R^2	SSR
PEI	1.205×10^{-3}	126.582	1	1.52×10^{-3}	125.393	0.99	11.561
PANI salt	3.01×10^{-3}	200.00	1	3.38×10^{-1}	198.64	0.99	0.0003

Table 4. Summary of adsorption parameters of the pseudo-first-order and Elovich models.

Polymer	Pseudo-First-Order Model			Elovich Model		
	q_e (mg/g)	K_1 (g/(mg.min))	R^2	β (g/mg)	α (mg/(g.min))	R^2
PEI	25.527	1.01×10^{-2}	0.93	0.21	1.97×10^{9}	0.87
PANI salt	5.90	4.60×10^{-3}	0.94	0.65	1.32×10^{53}	0.95

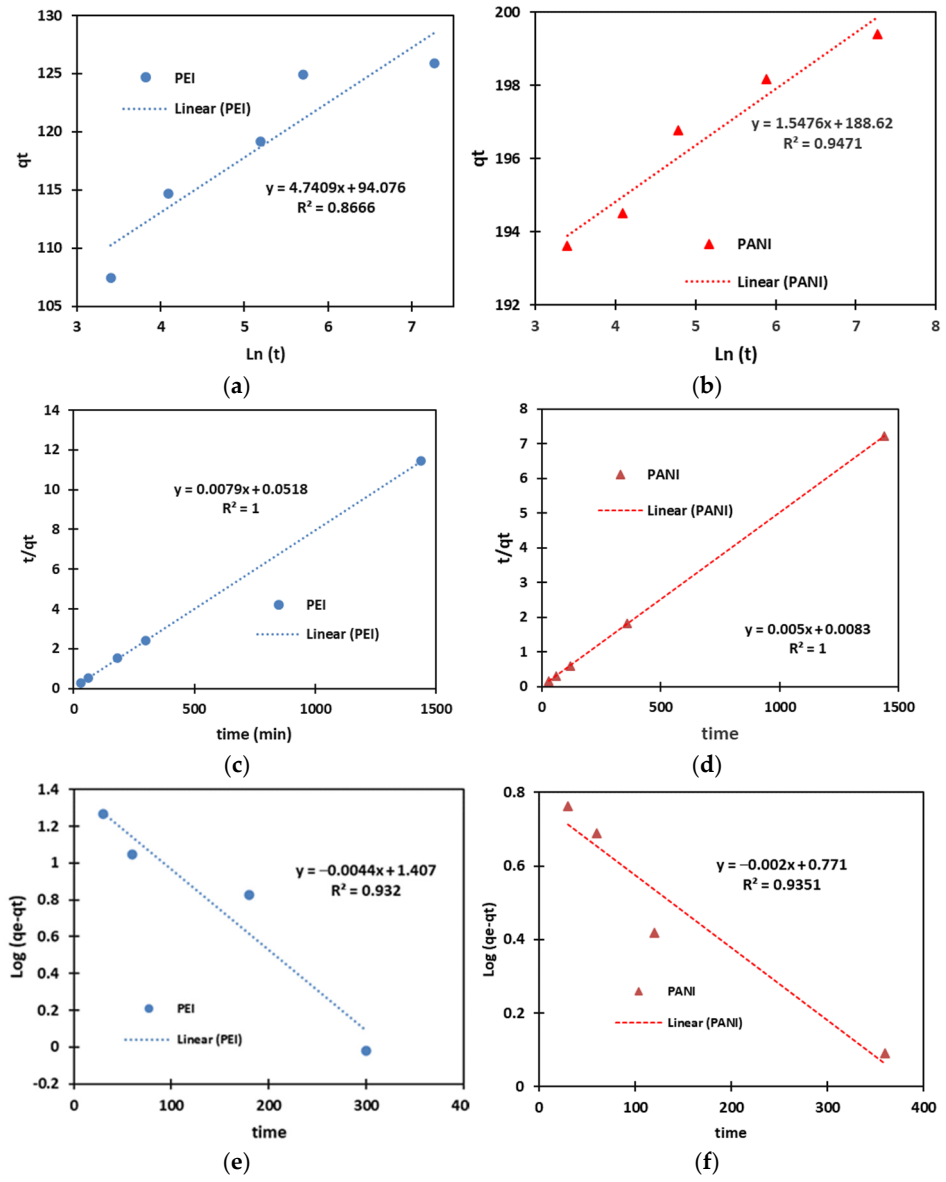


Figure 11. Elovich (**a**,**b**), pseudo-second-order (**c**,**d**), and pseudo-first-order (**e**,**f**) models.

As summarized in Table 4, the Elovich and pseudo-first-order theoretical models provided poor descriptions of the experimental data. The Elovich model (Figure 11a,b) yielded low R^2 values (0.947 and 0.866 for PANI and PEI), failing to explain the adsorption

of dichromate ions by the two polymeric materials. Similarly, the pseudo-first-order model (Figure 11e,f) exhibited deviation from linearity, implying that the adsorption kinetics do not follow a first-order rate law. In contrast, the pseudo-second-order model aligned perfectly with the experimental data. Plotting t/qt versus time (min) resulted in a perfect linear graph with the maximum possible R^2 value of 1.0 for both polymers, confirming that the adsorption process follows pseudo-second-order kinetics. The R^2 values from the nonlinearized pseudo-second-order model have resulted in 0.99 for both polymers. Similarly, the sum of squared residuals (SSR) was calculated to be 11.561 and 0.0003 for PEI and PANI salt, respectively. The lower SSR values are an additional confirmation of the success of the pseudo-second-order model in describing the dichromate adsorption kinetics of the two polymers. It should be noted that a pseudo-second-order adsorption model for dichromate with PANI salt (acid-doped PANI) has been reported in previous studies [47], which is consistent with our findings. Therefore, it indicates that the adsorption of the analytes primarily occurred via chemisorption (chemical bonding between the active functional groups of the adsorbent and the analyte) [48].

As expected, the theoretical and experimental adsorption value (qe) for PEI and PANI salt showed strong correlation using the linearized pseudo-second-order model. The calculated qe values (PEI: 126.582 mg/g; PANI salt: 200.000 mg/g) closely match the experimental equilibrium values (PEI: 125.860 mg/g; PANI salt: 199.406 mg/g), hence supporting the fact that this model is the best to explain the adsorption kinetics. The success of the pseudo-second-order model in predicting the adsorption process was also confirmed by fitting the experimental data in a nonlinearized equation (Equation (4)) [49], and the data points showed a perfect correlation (Figure 12 and Table 3).

$$q_t = \frac{K_2 q_e^2 t}{1 + K_2 q_e t} \tag{4}$$

The pseudo-second-order adsorption constant (K_2) and the amount of adsorbate per unit weight of adsorbent (mg/g) at equilibrium (qe) calculated from the nonlinearized fitting are 1.52×10^{-3} g/mg.min and 125.393 mg/g, respectively, for PEI. Similarly, K_2 and qe for the PANI adsorbent were calculated to be 3.39×10^{-1} g/mg.min and 198.642 mg/g, respectively. These values are very close to the data obtained from the linearized equation (Table 3). The closeness of the values of the linearized and nonlinearized formulas to each other and to the experimental data could be taken as confirmation that the pseudo-second-order model is indeed correct to describe the process of the adsorption of dichromate ions with PEI and PANI salt.

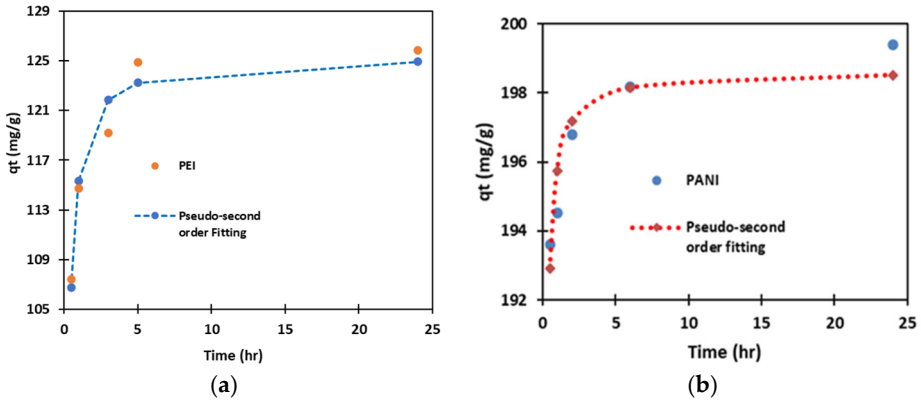


Figure 12. Fitting of the experimental data with a nonlinearized pseudo-second-order model: PEI (**a**) and PANI salt (**b**) (fitting was carried out using Excel Solver).

3.3. Adsorption Isotherms

Adsorption isotherms relate the concentration of an analyte, in this case dichromate, in the liquid phase and solid phase when the adsorption reaches equilibrium [50]. Hence, to gain a better understanding about the dichromate equilibrium concentration, a batch experiment was conducted at room temperature, where 10 mL of dichromate at different concentrations (250, 300, 350, and 400 ppm) was separately mixed with 0.015 g of the adsorbents (PEI) and 250, 300, 350, and 400 ppm (PANI salt) and agitated for 24 h. The concentration of the dichromate in the liquid phase (ce) from each of the mixtures was determined following the colorimetry method and UV–Visible spectroscopy. The UV–Visible absorption spectra of the solutions are given in Figures S4 and S5 (Supporting Information). The dichromate adsorbed (qe) in mg/g by the polymers was calculated based on the absorption spectrum and the calibration curve equation. The experimentally determined values were fitted on three theoretical adsorption isotherms (Langmuir, Freundlich, and Temkin) to determine the equilibrium adsorption capacity of the polymers and to evaluate other essential adsorption parameters.

The Langmuir model assumes a monolayer adsorption on the surface of the adsorbent, and its linear form is given in Equation (5). The quantities qm and k in the Langmuir equation represents the maximum adsorption capacity (mg/g) of the adsorbents and the affinity of the adsorbent to the analyte (L/mg), respectively [51,52].

$$\frac{c_e}{q_e} = \frac{1}{q_m k} + \frac{1}{q_m} c_e \quad (5)$$

A plot of ce/qe against ce (the equilibrium dichromate concentration) of the experimental data collected for the two polymers resulted in a linear graph, as shown in Figure 13a,b, where qm, k, and R^2 are determined from the graph and given in Table 5.

The experimental data were also fitted in the Freundlich isotherm model (linear form) given by Equation (6) [51,52].

$$\ln q_e = \ln k_f + \frac{1}{n} \ln c_e \quad (6)$$

A plot of ln q_e against ln c_e gave a linear equation (Figure 13c,d), where the model constants (kf and n) (Table 4) were obtained from the slope and the y-intercept of the graph, respectively. The Freundlich isotherm is developed with the assumption that both surface and multi-layer adsorption occur in the adsorption process [50].

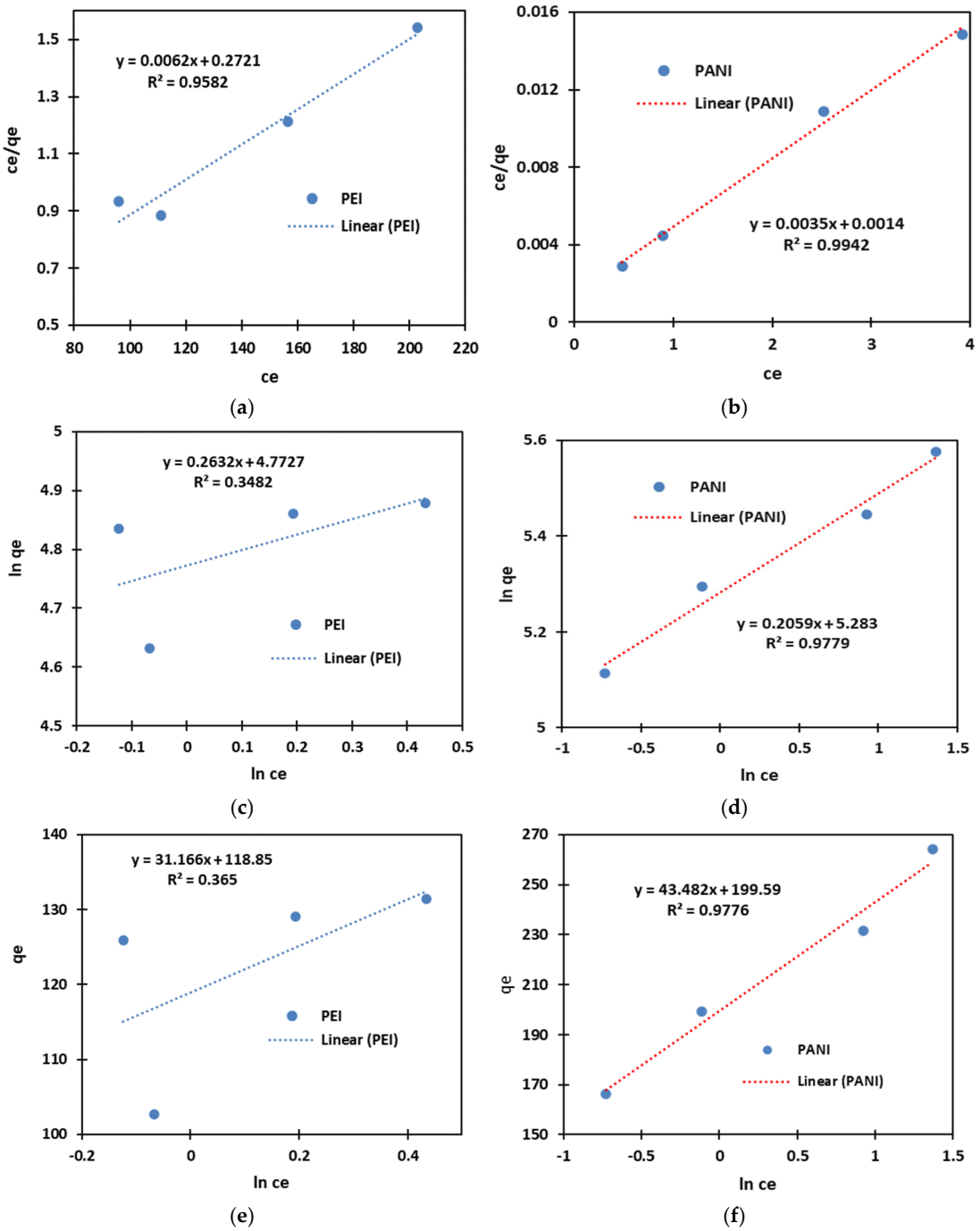
Equation (7) show the linear form of the Temkin isotherm [53,54], where qe and ce represent the mass of analyte adsorbed per unit mass adsorbent and the concentration of the analyte in the solution at equilibrium, respectively. The constant B_T is associated with adsorption heat and is expressed in units of J·mol^{-1}. The Temkin isotherm constant, A_T, corresponding to the maximum binding energy, is expressed in L·mg^{-1} [54]. R is the universal gas constant (8.314 J·mol^{-1}·K^{-1}), and T is the absolute temperature where the adsorption experiment was conducted [53]. The fitting of the experimental data to this model is shown in Figure 13e,f. The constants obtained are summarized in Table 5.

$$q_e = \frac{RT}{B_T} \ln A_T + \frac{RT}{B_T} \ln c_e \quad (7)$$

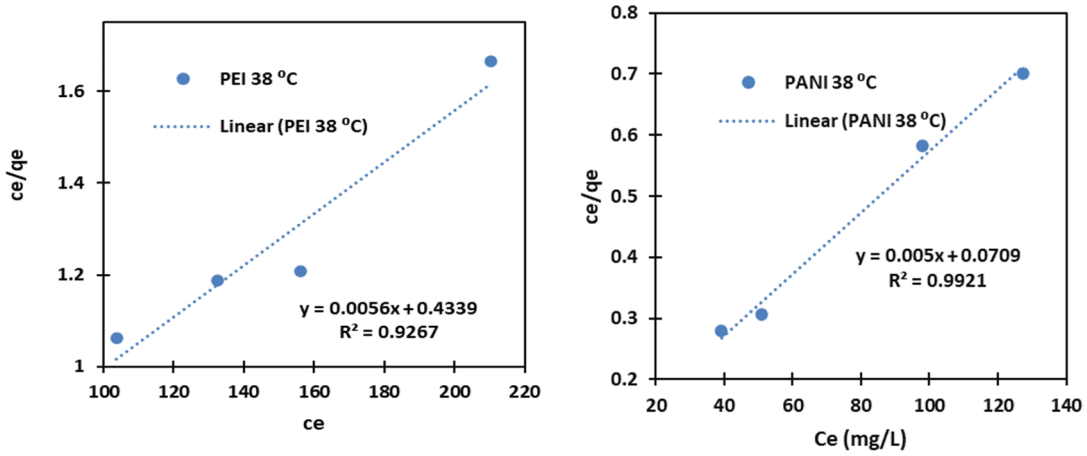
Table 5 summarizes the Langmuir, Freundlich, and Temkin isotherm model adsorption parameters for PEI and PANI salt. It was found that the R^2 values were higher in the Langmuir model (R^2 = 0.958 for PEI and R^2 = 0.994 for PANI salt) compared to the corresponding values obtained using the Freundlich model (R^2 = 0.348 for PEI) and the Temkin model (R^2 = 0.365 for PEI and R^2 = 0.978 for PANI). The Freundlich and Temkin models, however, resulted in relatively higher R^2 values for PANI salt as opposed to PEI. The higher R^2 values in the Langmuir model means that the adsorption of dichromate on PEI and PANI prefers the Langmuir model to the Freundlich and Temkin models.

Table 5. Linear adsorption isotherm parameters (Langmuir, Freundlich, and Temkin).

Polymer	Langmuir Model			Freundlich Model			Temkin Model		
	qm (mg/g)	k (L/mg)	R^2	Kf (L/mg)	n	R^2	B_T (J/mol)	AT (L/mg)	R^2
PEI	161.290	0.002	0.958	118.238	3.799	0.348	79.496	-	0.365
PANI salt	285.714	2.500	0.994	196.960	4.856	0.978	56.979	98.511	0.978



https://doi.org/10.3390/app162110916



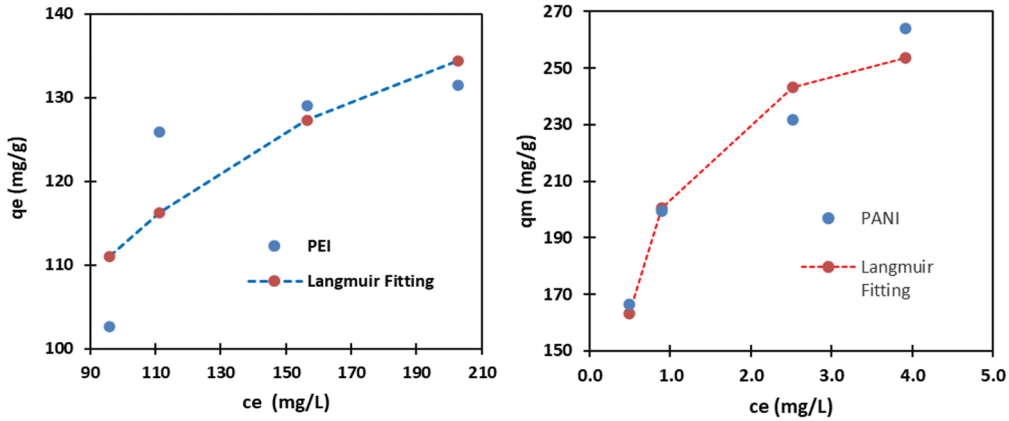
(**g**) (**h**)

Figure 13. Dichromate adsorption isotherms of PEI and PANI: Langmuir (**a**,**b**); Freundlich (**c**,**d**); Temkin (**e**,**f**); Langmuir at 38 °C (**g**,**h**).

The experimental adsorption isotherms were also fitted in nonlinear Langmuir (Equation (8)), Freundlich (Equation (9)), and Temkin (Equation (10)) adsorption models. The Langmuir and Temkin models are shown in Figure 14, and the constants are summarized in Table 6, while the Freundlich model and corresponding constants are given in the Supporting Information Figure S6 and Table S1.

Table 6. Nonlinear adsorption isotherm parameters (Langmuir and Temkin) (fitting was carried out using Excel Solver).

Polymer	Nonlinear Langmuir Model			Nonlinear Temkin Model		
	qm (mg/g)	k (L/mg)	SSR	b_T (mg/g)	K_T (L/mg)	SSR
PEI	165.815	0.021	173.278	31.397	0.362	189.959
PANI salt	275.203	3.021	251.319	43.482	98.510	118.664



(**a**) (**b**)

https://doi.org/10.3390/app162110916

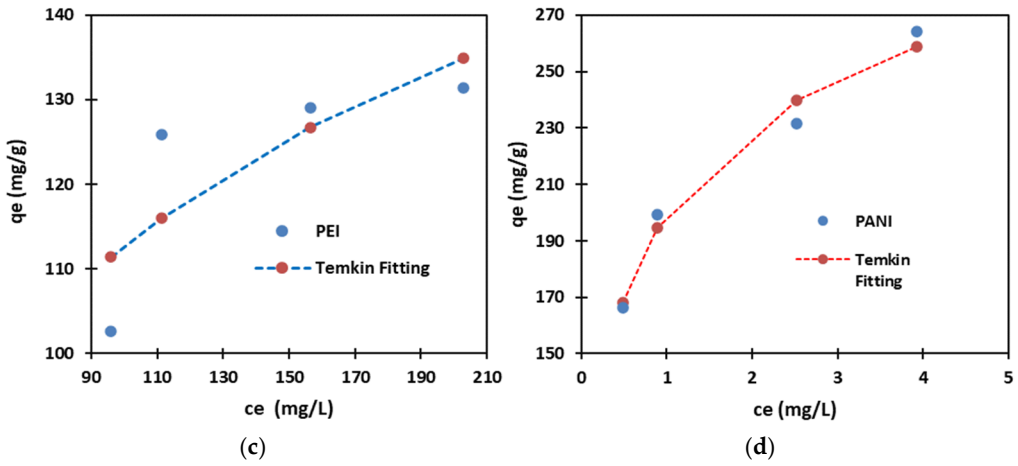


Figure 14. Dichromate adsorption isotherms of PEI and PANI using the nonlinear Langmuir (**a**,**b**) and Temkin (**c**,**d**) models (fitting was carried out using Excel Solver).

$$q_e = \frac{q_m . k . c_e}{1 + k . c_e} \quad (8)$$

$$q_e = K_F . c_e^{1/n} \quad (9)$$

$$q_e = b_T \ln(A_T . C_e) \quad (10)$$

At room temperature, the maximum equilibrium dichromate adsorption capacities (qm) calculated from the linear Langmuir model were 161.290 mg/g for PEI and 285.714 mg/g for PANI. The nonlinear fitting of the same model yielded adsorption capacities of 165.815 mg/g and 275.203 mg/g, respectively, which are highly comparable to the values obtained from the linear approach. Notably, these equilibrium capacities are significantly higher than those derived from the linear pseudo-second-order kinetic model (126.582 mg/g for PEI and 200.00 mg/g for PANI). The corresponding nonlinear kinetic capacities were 125.393 mg/g for PEI and 198.642 mg/g for PANI salt; these lower values stem from the use of a single initial dichromate concentration (300 ppm), which underestimates the true maximum thermodynamic adsorption capacity. The other constant extracted from the Langmuir model is k, which is related to the strength of the affinity of the analyte to the adsorbent. A k value for PEI (0.002 L/mg) and PANI (2.500 L/mg) was obtained. The corresponding values from the nonlinear model are 0.021 L/mg and 3.021 L/mg. The nonlinear and linear Temkin model provided the constants (b_T and A_T) and are given in Tables 5 and 6. The sum of squared residuals (SSR) from the nonlinear fitting was smaller for PEI in the Langmuir model but higher in the Temkin model relative to the values of the PANI salt adsorbent.

A comparison of dichromate adsorption capacity of materials reported in the literature are shown in Table 7. Indeed, PEI and PANI salt are among the promising materials for capturing dichromate from contaminated water.

Table 7. Comparative evaluation of Cr^{6+} adsorbent materials from the literature.

Dichromate Adsorbent Materials	Adsorption Capacity (mg g^{-1})	Ref
MOF Cd(tipo)(HCOO)(H_2O)].NO_3.DMF tipo=tris(4-(1H-imidazol-1-yl)phosphine oxide)	228.00	[55]
DTU-52	120.68	[56]
Ferric coordinated [3-(2-aminoethylamino)propyl] trimethoxysilane–MCM-41	84.90	[57]

Manihot esculenta leaf extract-mediated silver–clay nanocomposite	137.91	[58]
Fe_3O_4/G/PANI composite containing magnetite nanoparticles (Fe_3O_4), graphene sheets (G), and polyaniline (PANI)	153.54	[34]
Biochar prepared from coconut shells	4.72	[15]
Polyaniline nanofibers	142.85	[59]
Cationic porous organic polymer (POP) (PTPA–PIP)	230	[60]
Polyethylenimine-functionalized poly(vinyl alcohol) (PEI-PVA)	396.83	[26]
PEI microgel, cryogel, and bulkgel	84.7 ± 0.8, 76.5 ± 5.2, 108.9 ± 2.4	[61]
Polyaniline doped with sulfuric acid	95.79	[47]
Glutaraldehyde-crosslinked PEI (linear Langmuir)	161.290	This work
PANI salt (linear Langmuir)	285.714	This work

3.4. Adsorption Thermodynamics

The thermodynamic properties of the adsorption process were also investigated. In this case, 10 mL each of the 250, 300, 350, and 400 ppm of dichromate solutions was mixed with 0.015 g of PEI and 0.015 g PANI salt and left at room temperature (28 °C) and at a higher temperature (38 °C) in a water bath shaker for 24 h. A 2 mL aliquot of each of the solutions (the filtrate from PEI were diluted at a 1:35 ratio) was mixed with the required reagents (0.2 mol/L H_2SO_4 and 0.5% *w*/*v* 1,5-diphenyl carbazide in acetone). Notably, the PANI salt demonstrated a lower binding affinity for dichromate at the elevated temperature. According to the linear Langmuir model, the qm of the PANI salt decreased to 200 mg/g at 38 °C (Figure 13h) from the 285 mg/g recorded at room temperature. This inverse temperature dependence suggests that the update of dichromate by the PANI salt is primarily driven by exothermic electrostatic attractions between the positively charged polymer backbone and the anionic dichromate species, a mechanism that becomes thermodynamically less favorable at higher temperatures. PEI, on the other hand, absorbs dichromate at 38 °C at a comparable tendency when compared to its capacity at room temperature (28 °C). In fact, a Langmuir linear model treatment of the adsorption of PEI at 38 °C (Figure 13g) gave a maximum adsorption capacity (qm) of 178.571 mg/g. This result can be taken as evidence for the presence of more than one adsorption mechanism operating in PEI. PEI, being a nitrogen-rich material, could have a strong interaction with the analyte, such as chelation, which is stable at higher temperature (38 °C). The UV–Visible absorption spectra of purple-colored samples (after 35-fold dilution) for PEI- and PANI salt-treated samples were recorded, and the results obtained are shown in Figure S7, Supporting Information. Following the standard procedure reported in the literature, [50,62–65], the equilibrium constant (K^o) at the two working temperatures was calculated for the PEI and PANI salt dichromate adsorbents. The concentration of the dichromate adsorbed by PEI/PANI salt at equilibrium (cs) and the concentration of the dichromate remaining in the liquid phase at equilibrium (ce) were calculated from the UV–Visible absorption spectra. The ratio of cs to ce is taken as the equilibrium constant at the two temperatures and is given in Table 8. A plot of ln(cs/ce) against ce gave a linear graph (Figure 15), which is used in the calculation of the equilibrium constants.

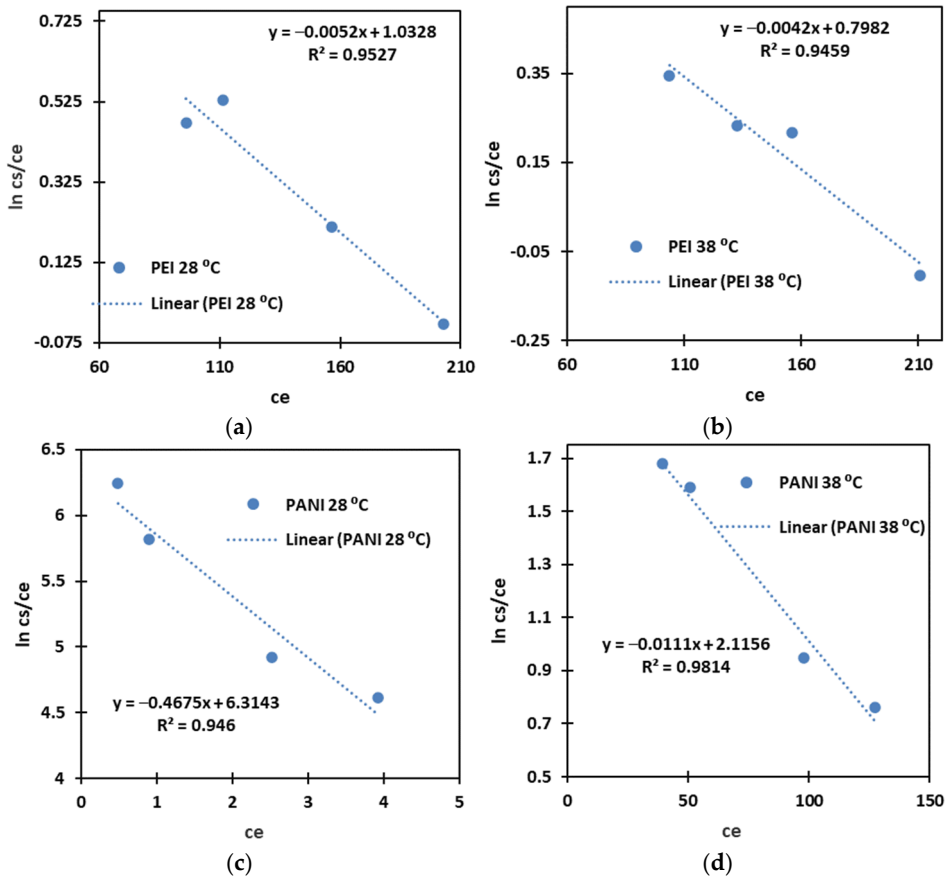


Figure 15. Plot of ln(cs/ce) versus ce for dichromate on PEI and PANI salt: (**a**) PEI at 28 °C; (**b**) PEI at 38 °C; (**c**) PANI at 28 °C; (**d**) PANI at 38 °C.

The equilibrium constants at 28 °C and 38 °C for PEI were calculated, by extrapolating the linear graphs (Figure 15a,b), to be 2.809 and 2.222, respectively. A similar calculation for PANI salt (Figure 15c,d) resulted in equilibrium constants of 552.413 and 8.295 at 28 °C and 38 °C, respectively. A decrease in K° values with an increase in the absolute temperature for both materials is an indication that the adsorption processes prefer lower temperatures.

The standard Gibbs free energy (ΔG°) (Table 8) was calculated using Equation (11), where R is the universal gas constant (8.314 J/mol·K), T is the absolute temperature, and K° is the thermodynamic equilibrium constant. For PEI, a negative standard Gibbs free energy of −2584.595 J/mol and −5744.127 J/mol was obtained at 301 K (28 °C) and 311 K (38 °C), respectively. The corresponding ΔG° values for PANI salt were −15,801.614 J/mol and −5470.206 J/mol at the respective temperatures. The negative magnitudes of ΔG° across all conditions confirm that the adsorption processes on both polymers' matrices are thermodynamically spontaneous.

$$\Delta G^\circ = -RT \ln K^\circ \quad (11)$$

The other thermodynamic quantity of relevance is the standard enthalpy change (ΔH°), which can be calculated by using the Van't Hoof equation (Equation (12)) [63]. The change in enthalpy for PEI was calculated to be −18,258.480 J/mol, while that of the PANI salt was calculated to be −326,776.982 J/mol, which supports the exothermic nature of the adsorptions.

$$\ln\left[\frac{K^\circ 1}{K^\circ 2}\right] = -\frac{\Delta H^\circ}{R}\left[\frac{1}{T_1} - \frac{1}{T_2}\right] \quad (12)$$

Using the ΔG°, T, and ΔH° values provided above, the change in entropy (ΔS°) was calculated to be −40.239 J/mol.K (PEI) and −1033.141 J/mol.K (PANI salt) using Equation

(13). A negative change in enthalpy and negative change in entropy means that the adsorption will be spontaneous at lower temperatures.

$$\Delta G° = \Delta H – T\Delta S° \quad (13)$$

Table 8. A summary of thermodynamic properties of the adsorption of dichromate with PEI.

Polymers	K°		ΔG° (J/mol)		ΔH° (J/mol)	ΔS° (J/mol.K)
	28 °C	38 °C	28 °C	38 °C		
PEI	4.181	3.402	−2584.595	−5744.127	−18,258.480	−40.239
PANI salt	552.413	8.295	−15,801.614	−5470.206	−326,776.982	−1033.141

3.5. Effect of the Presence of Other Ions on the Adsorption of Dichromate

The tolerance of the 1,5-diphenylcarbazide-based coulometric method for dichromate measurement in the presence of three salts ($NaNO_3$, KH_2PO_4, and $CuSO_4$) was evaluated. Lace et al. [37] previously reported that this coulometric method is not affected by the presence of 100 ppm PO_4^{3-} and 10 ppm NO_3^- in a 1 ppm dichromate solution. In the present study, the UV absorption intensity of a 6 ppm dichromate solution mixed with 6 ppm $NaNO_3$, 6 ppm KH_2PO_4, 1 ppm $CuSO_4$, or 3 ppm $CuSO_4$ was found to be comparable with that of the 6 ppm dichromate control solution. Specifically, the decrease in absorbance intensity relative to the control was 0.088%, 3.222%, 0.834%, and 1.259% for 6 ppm $NaNO_3$, 6 ppm KH_2PO_4, 1 ppm $CuSO_4$, and 3 ppm $CuSO_4$, respectively. These results imply that the coulometric method can be employed to quantify the dichromate adsorption capacity of the two adsorbent materials in the presence of equal concentrations of $NaNO_3$ and KH_2PO_4. On the other hand, the tolerable concentration of $CuSO_4$ for the coulometric method is half that of the dichromate, as an increase in the concentration of the added salts generally reduces the absorbance peak by more than ~3%. To assess the adsorption capacity of the adsorbents, three separate 300 ppm dichromate solutions containing 300 ppm KH_2PO_4, 300 ppm $NaNO_3$, and 150 ppm $CuSO_4$ were prepared. A 10 mL sample of each of the solutions was shaken with 0.015 g of PEI or PANI salt for 24 h. The dichromate adsorption efficiency (%) was evaluated, and the results are shown in Table 9. Evidently, the adsorption efficiency of PEI was negatively affected by the presence $NaNO_3$ and $CuSO_4$, yielding a slightly lower dichromate adsorption efficiency of 53.350% and 51.856%, respectively. In contrast, the PEI selected dichromate over KH_2PO_4; in this case, the dichromate adsorption efficiency was comparable to that of the control (~62.930%). The PANI adsorbent, conversely, demonstrated a high selectivity for dichromate ions over the other added salts, maintaining a strong preference for dichromate.

Table 9. Effect of presence of other ions on the dichromate removal efficiency of PEI and PANI salt.

PEI		PANI Salt	
Salt Added to 300 ppm $Cr_2O_7^{2-}$	**% Adsorption of $Cr_2O_7^{2}$**	**Salt Added to 300 ppm $Cr_2O_7^{2-}$**	**% Adsorption of $Cr_2O_7^{2-}$**
None	62.930	None	99.592
300 ppm KH_2PO_4	65.115	300 ppm KH_2PO_4	99.118
300 ppm $NaNO_3$	53.350	300 ppm $NaNO_3$	99.029
150 ppm $CuSO_4$	51.856	150 ppm $CuSO_4$	93.863

3.6. Reusability of Crosslinked PEI and PANI Salt for Adsorption of Dichromate

Another key factor for the sustainable use of adsorbents is the regeneration process [66,67]. Several studies have shown that both PEI and PANI salt adsorbents can be effectively regenerated for reuse using acid and base treatments. Kubilay et al. reported the successful regeneration of PEI microgel using 1 mol/L HCl (up to 5 times) in a successive adsorption/desorption experiment [61]. The used PANI can also be recycled by using acids and bases [29]. In this study, desorption experiments were conducted to evaluate the potential regeneration of both PEI and PANI salt. The two polymers (0.065 g each) were loaded with 10 mL of 100 ppm dichromate solution with agitation for 24 h. The difference between the UV–Visible spectrum of the polymer-treated dichromate samples and the 10 ppm untreated standard dichromate clearly shows the dichromate ions were effectively eliminated from the solutions (Figure S8, Supporting Information).

The dichromate adsorbed polymers were filtered separately and washed extensively with deionized water to remove any unbound dichromate ions. The dichromate-loaded polymers were dried at room temperature overnight and then treated with 10 mL of 1 mol/L HCl and 1 mol/L NaOH in a centrifuge tube and agitated on a shaker for 4 h. The amount of desorbed dichromate ions in the resulting liquid phase was quantified after appropriate dilution using atomic absorption spectroscopy (AAS), employing the calibration curve. The percentage of desorbed dichromate is shown in Figure 16 (note that the calibration curve used for the calculation of desorbed dichromate is described by the equation $y = 0.0106x + 0.0202$) (Figure S9, Supporting Information). It is important to note that the total chromium was monitored via AAS, as the potential reduction of Cr^{+6} to lower oxidation states would otherwise obscure individual species quantification.

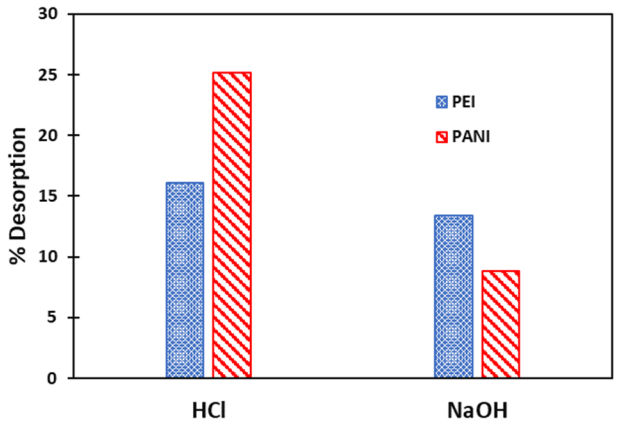


Figure 16. Desorption of dichromate from PEI and PANI salt using 1 mol/L HCl and 1 mol/L NaOH.

It should be noted that desorption experiments using 1 mol/L HCl and 1 mol/L NaOH revealed that only a low percentage (8–25%) of the adsorbed dichromate ions were successfully eluted after the acid and base treatments of the polymers. The desorption rates reached 16% with PEI and 25% with PANI using the acid treatment, outperforming the 1 mol/L NaOH treatment, which achieved only 13% and 9% desorption, respectively. Therefore, HCl proved to be a relatively more effective desorbing agent than NaOH. The regeneration of the polymer might also be improved by repeating the desorption process with fresh solvent. Given the low observed desorption efficiency, we explored the recyclability of the polymers using 5% HNO_3 instead as a dichromate eluent. It is to be noted that 2% HNO_3 proved to be efficient to desorb ions (Cu^{2+}) from PEI [24,25] in past studies. Like the above study, the polymers (PEI = 0.0147 g and PANI = 0.0425 g) were loaded with dichromate from 10 mL of 300 ppm and 10 mL of 600 ppm dichromate

solutions, respectively. Desorption of the dichromate was achieved by shaking the dichromate-loaded polymers in 20 mL of 5% HNO_3 for 24 h. The eluent was decanted after centrifugation for 15 min at 3000 rpm, and subsequently, the solids were washed three times with 25 mL of DI water each time by centrifuging for 15 min at 3000 rpm and replacing with fresh DI water. The polymers were then used for a subsequent adsorption experiment, and the process was repeated four times. Each time, the dichromate removal efficiency of the recovered polymers was assessed following the coulometric method, and the result is shown in Figure 17. It is interesting to observe that PANI salt showed a removal efficiency of above 98% from 600 ppm for three consecutive adsorptions, while the fourth attempt gave a removal efficiency of a respectable 94% efficiency. This result clearly shows that PANI salt is quite stable for as many as four rounds of desorption with 5% HNO_3 and subsequent adsorptions. On the other hand, the first adsorption efficiency of PEI was 88.790%, which is slightly lower than the subsequent three adsorption trails, which increased to 99%. It is important to remember that crosslinked PEI was synthesized in water and under neutral pH, and the concentration of protonated nitrogen could be small; hence, the electrostatic interaction with dichromate is expected to be limited. However, the first acid treatment for the released dichromate might have left the nitrogen atoms protonated, hence improving the dichromate removal efficiency via electrostatic interaction.

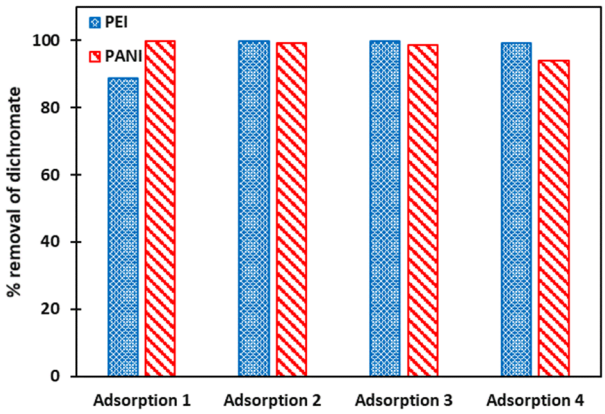


Figure 17. Recyclability of PEI (**dotted**) and PANI salt (**stripped**) using 5% HNO_3 as the eluent of dichromate.

The recyclability of the two adsorbent materials was also evaluated using AAS. Experiments were conducted using 0.04 g of each polymer and 10 mL of a 600 ppm dichromate solution with agitation for 24 h. The adsorbed dichromate was subsequently eluted using 20 mL of 5% HNO_3, and the remaining solids were washed three times with deionized (DI) water prior to successive adsorption–desorption cycles. Table 10 and Figures S10, Table S2 and S11 summarize the adsorption/desorption efficiencies, raw AAS data snippets, and the calibration curves, respectively. For the PANI salt, the adsorption and desorption efficiencies across the first three cycles ranged between 94 and 98% and 75 and 87%, respectively. In contrast, PEI exhibited a lower adsorption efficiency in the first cycle (64%), which then rose to 100% in cycles 2 and 3, respectively. This initial upward trend in adsorption efficiency aligns with our colorimetric observations (Figure 17). We ascribe this behavior to the protonation of the PEI amine groups during the first desorption step, which enhanced the material's affinity to interact with dichromate ions in subsequent cycles. Overall, the desorption efficiency of dichromate from PEI across the three cycles ranged from 61 to 93%, demonstrating that both materials possess excellent recyclability.

Table 10. Adsorption–desorption of dichromate from PEI and PANI salt using 5% HNO_3 and evaluated with AAS (PEI adsorption 1 was diluted at a 1:100 ratio, while the rest were diluted at a 1:25 ratio for AAS; all desorption experiments were carried out in 20 mL of 5% HNO_3 and then diluted at a 1:100 ratio for AAS).

	Adsorption Cycle	Absorbance (Corrected)	Unadsorbed (ppm)	Adsorbed (ppm)	Adsorption Efficiency (%)
PEI	Ads 1	0.032	212.214	387.786	64.631
	Ads 2	0.001	−6.489	606.489	101.081
	Ads 3	0.006	1.908	598.092	99.682
PANI salt	Ads 1	0.023	34.733	565.267	94.211
	Ads 2	0.009	8.588	591.412	98.569
	Ads 3	0.019	26.908	573.092	95.515
	Desorption Cycle	**Absorbance (Corrected)**	**Desorbed (ppm) (×100 Diluted)**	**Desorbed (ppm) (in 10 mL)**	**Desorption Efficiency (%)**
PEI	Des 1	0.020	1.191	238.168	61.417
	Des 2	0.033	2.145	429.008	70.736
	Des 3	0.041	2.794	558.779	93.427
PANI salt	Des 1	0.037	2.450	490.076	86.698
	Des 2	0.034	2.214	442.748	74.863
	Des 3	0.035	2.305	461.069	80.453

3.7. Comparison of the FTIR of Pristine and Dichromate-Loaded Materials

Regarding the reaction mechanism, previous studies have proposed four steps for PANI-modified adsorbents (nanofiber mats and membranes, PANI/bio-adsorbents, and PANI/magnetic) of dichromate involving electrostatic attraction of Cr^{6+} to the ionic PANI chain, anion exchange of Cl^- (when the PANI salt is a chloride) with Cr^{6+}, the reduction of Cr^{6+} to Cr^{3+}, and the chelation of the Cr^{3+} by the polymer chains [29,68]. In contrast, the adsorption mechanism of crosslinked PEI is expected to involve two primary interactions: electrostatic attraction and chelation. The strong electrostatic attraction between the protonated nitrogen of the crosslinked materials and the anionic dichromate ions facilitates the adsorption process. As for chelation, the nitrogen atoms in the amine groups of PEI can also act as electron-donating sites to chelate or bind with the species. The IR spectra of the polymers and polymer–dichromate solids are compared in Figure 18. The IR peak appearing at 1300 cm^{-1} in PANI salt is assigned to C–N stretching of a secondary aromatic amine. Similarly, a carbon-protonated nitrogen (C–N^+) stretching band in the PANI salt occurs at 1242 cm^{-1} [69,70]. Both peaks have either diminished in intensity or shifted to 1316–1341 cm^{-1} in the chromium-containing salt (PANI–Cr). In addition, a strong broad band in the range of 1110−1160 cm^{-1} is assigned to vibration of the protonated imine (Q = NH^+–B) or the polaron lattice of PANI (B–NH+–B) (where Q and B are for quinoid and benzoid forms of the ring) [70,71] in both PANI and PANI-Cr. On the other hand, the IR spectra of PEI and PEI–Cr are more or less similar in the pattern except that the intensity of the bands in PEI–Cr is generally weaker. For example, C-N stretching (~1270–1300 cm^{-1}) has almost disappeared in the PEI–Cr. C=N stretching (~1640 cm^{-1}) and primary amines [72] (~1560 cm^{-1}) are both in the PEI–Cr IR spectra compared to that of PEI.

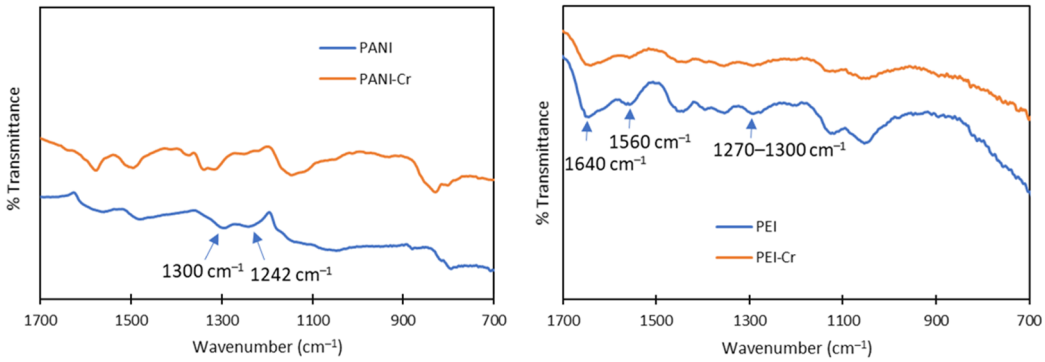


Figure 18. Comparison of the IR spectra: PANI salt and PANI salt–Cr; PEI and PEI–Cr.

3.8. Thermogravimetric Analysis (TGA) Comparison of PEI, PANI Salt, and Dichromate-Loaded Adsorbents

The thermal stability of PEI, PANI salt, and their dichromate-loaded versions were investigated using TGA from 300 °C to 600 °C in a nitrogen atmosphere (Figure 19). In the experiment, the samples were kept at 300 °C for 1 min and then heated at a 25 °C/min rate. It was observed that 3% of the mass of PEI and PEI-Cr was already lost during the 1 min of heating at 300 °C, and the weight decreased quickly as the temperature increased, with half of the mass decomposing at ~425–435 °C, which indicates the lower stability of both PEI and dichromate-loaded PEI at high temperatures. At 450 °C, 35% of the PEI and 26% of the PEI-Cr are left. As opposed to the former material, the masses of PANI and PANI-Cr are stable, with less than 2% mass lost during the initial 1 min of heating at 300 °C. With further increases in the temperature, PANI salt showed a decrease in its mass at a slower pace compared to that of PEI. At 450 °C, 40% of the mass of PANI salt-Cr remained, while the mass of PANI left at the same temperature was 89%. Like PEI-Cr, PANI-Cr also has a higher mass as compared to PANI, which could be attributed to the decomposition of the dichromate at ~450 °C, which will release oxygen, which is likely to facilitate the decomposition of the host polymeric material at a faster rate. On the other hand, both PANI and PANI-Cr are more stable at higher temperatures compared to the corresponding PEI and PEI-Cr, respectively.

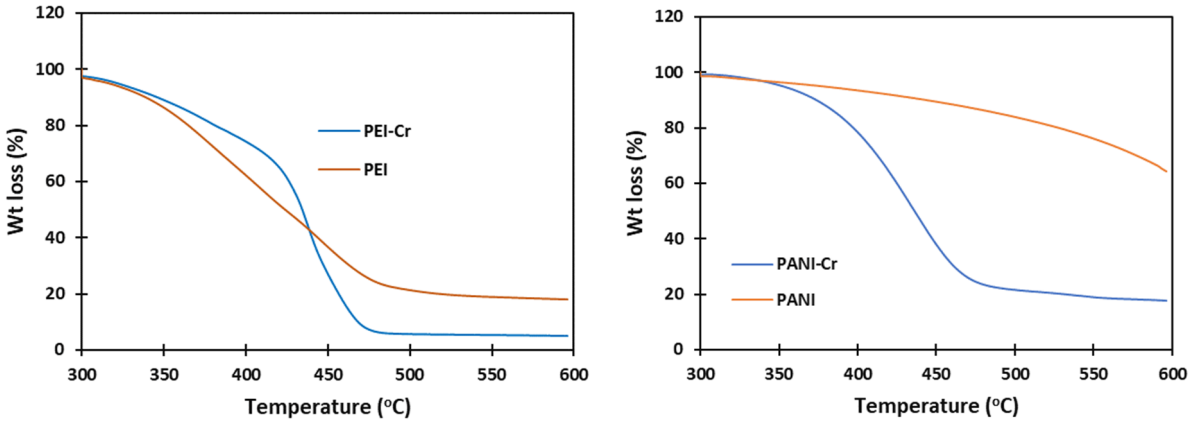


Figure 19. TGA of PEI, PANI salt, PEI–Cr, and PANI salt–Cr.

4. Conclusions

The present study demonstrates that glutaraldehyde-crosslinked polyethylene imine (PEI) and polyaniline (PANI) salt are effective, easily synthesized materials for highly efficient dichromate remediation.

https://doi.org/10.3390/app162110916

- Both adsorbents achieved remarkable removal efficiencies of ~99% (PANI salt) and 49–62% (PEI) from 250 to 400 ppm diluted dichromate solutions within 24 h of agitation.
- The linear Langmuir adsorption isotherms provided an adsorption capacity of ~161.290 mg/g and ~285 mg/g for PEI and PANI salt, respectively.
- The dichromate adsorption capacity decreases with an increase in temperature, likely due to the unstable nature of the ion pair formed between the adsorbents and the analyte.
- These findings suggest that both crosslinked PEI and PANI salt possess significant potential for practical, real-life application in treating water sources contaminated with Cr^{6+}.
- Future studies should leverage a wider range of analytical techniques, such as X-ray photoelectron spectroscopy (XPS), Raman spectroscopy, Nuclear Magnetic Resonance (NMR) spectroscopy, and Brunauer–Emmett–Teller (BET) surface area analysis, on top of the analytical techniques reported in our work to more deeply evaluate the material properties and unequivocally elucidate the dichromate adsorption mechanisms of these two adsorbents.

Supplementary Materials: The following supporting information can be downloaded at: https://www.mdpi.com/article/10.3390/app162110916/s1, Figure S1: Polymer pictures a) Glutaraldehyde-crosslinked PEI; b) PANI salt; c) PANI base (washed with 0.2 mol/L NaOH); Figure S2: UV-Visible absorption spectra of dichromate standards (2–10 ppm) and calibration curve; Figure S3: UV-Visible absorption of 0.015 g of PEI and PANI salt treated 300 ppm dichromate solution over 24 h time; Figure S4: UV-Visible absorption spectra of PEI treated 250, 300, 350 and 400 ppm dichromate for adsorption isotherms (Langmuir, Freundlich and Temkin) (28 °C); Figure S5: UV-Visible absorption spectra of PANI salt treated 250, 300, 350 and 400 ppm dichromate for adsorption isotherms (Langmuir, Freundlich and Temkin) (28 °C); Figure S6: Dichromate adsorption isotherms of PEI and PANI salt using the nonlinear Freundlich model (Fitting was carried out using Excel Solver); Figure S7: UV-Visible absorption spectra of 0.015 g PEI/ PANI salt treated 10 mL 250, 300, 350 and 400 ppm dichromate at 38 °C for 24 h; Figure S8: UV-Visible absorption of 0.065 g of PEI and PANI salt treated with 100 ppm dichromate solution for 24 h and 10 ppm untreated dichromate standard solution (for comparison); Figure S9: Calibration curve from AAS to calculate desorbed dichromate; Table S1: Summary of nonlinear Freundlich model ((Fitting was carried out using Excel Solver); Figure S10: Snippet of the dichromate adsorption and desorption study from the AAS; Table S2: AAS calibration curve values for adsorption-desorption analysis; Figure S11: AAS calibration curve for adsorption-desorption analysis.

Author Contributions: Conceptualization, D.G.; methodology, T.T. (Thomas Tunidau), A.C., X.P., M.R.A., and D.G.; software, T.T. (Thomas Tunidau), T.T. (Taitusi Taufa), and X.P.; validation, T.T. (Thomas Tunidau), A.C., T.T. (Taitusi Taufa), A.A.S., F.S.M., X.P., M.R.A., and D.G.; formal analysis, T.T. (Thomas Tunidau), A.C., T.T. (Taitusi Taufa), A.A.S., F.S.M., X.P., M.R.A., and D.G.; investigation, T.T. (Thomas Tunidau), A.C., T.T. (Taitusi Taufa), A.A.S., F.S.M., X.P., M.R.A., and D.G.; writing—original draft preparation, D.G.; writing—review and editing, T.T. (Thomas Tunidau), A.C., T.T. (Taitusi Taufa), A.A.S., F.S.M., X.P., M.R.A., and D.G.; supervision, T.T. (Taitusi Taufa), A.A.S., F.S.M., X.P., M.R.A., and D.G. All authors have read and agreed to the published version of the manuscript.

Funding: This research received no external funding.

Data Availability Statement: The original contributions presented in this study are included in the article/Supplementary Material. Further inquiries can be directed to the corresponding author.

Acknowledgments: We wish to thank the Discipline of Biological and Chemical Sciences and School of Agriculture, Geography, Environment, Ocean and Natural Sciences, USP, for generously providing the necessary chemicals and instruments used in this study. The authors acknowledge the facilities and the scientific and technical assistance of Microscopy Australia (ROR: https://ror.org/042mm0k03), enabled by NCRIS and the government of South Australia at Flinders Microscopy and Microanalysis (ROR: https://ror.org/04z91ja70), Flinders University (ROR: https://ror.org/01kpzv902).

Conflicts of Interest: The authors declare no conflicts of interest.

References

1. Kozlowski, H.; Janicka-Klos, A.; Brasun, J.; Gaggelli, E.; Valensin, D.; Valensin, G. Copper, iron, and zinc ions homeostasis and their role in neurodegenerative disorders (metal uptake, transport, distribution and regulation). *Coord. Chem. Rev.* **2009**, *253*, 2665–2685. https://doi.org/10.1016/j.ccr.2009.05.011.
2. Andersson, C.V.I.; Mudiyanselage, S.G.T.; Peeks, M.D.; Kroeger, A.A.; Virtue, J.I.; Mann, M.; Chalker, J.M.; Coote, M.L.; Johnston, M.R.; Bloch, W.M. Efficient Removal of Short-Chain Perfluoroalkyl Substances by Cavity-Directed Aggregation in a Molecular Cage Host. *Angew. Chem. Int. Ed.* **2026**, *65*, e26027. https://doi.org/10.1002/anie.202526027.
3. Acioly, T.M.d.S.; da Silva, M.F.; Barbosa, L.A.; Iannacone, J.; Viana, D.C. Levels of Potentially Toxic and Essential Elements in Water and Estimation of Human Health Risks in a River Located at the Interface of Brazilian Savanna and Amazon Biomes (Tocantins River). *Toxics* **2024**, *12*, 444. https://doi.org/10.3390/toxics12070444.
4. Acosta, R.I.; Rodríguez, X.; Gutiérrez, C.; Moctezuma, M.d.G. Biosorption of Chromium (VI) from Aqueous Solutions onto Fungal Biomass. *Bioinorg. Chem. Appl.* **2004**, *2*, 486496. https://doi.org/10.1155/S1565363304000019.
5. Hamadi, N.K.; Chen, X.D.; Farid, M.M.; Lu, M.G.Q. Adsorption kinetics for the removal of chromium(VI) from aqueous solution by adsorbents derived from used tyres and sawdust. *Chem. Eng. J.* **2001**, *84*, 95–105. https://doi.org/10.1016/S1385-8947(01)00194-2.
6. Famielec, S. Chromium Concentrate Recovery from Solid Tannery Waste in a Thermal Process. *Materials* **2020**, *13*, 1533. https://doi.org/10.3390/ma13071533.
7. Kimbrough, D.E.; Cohen, Y.; Winer, A.M.; Creelman, L.; Mabuni, C. A Critical Assessment of Chromium in the Environment. *Crit. Rev. Environ. Sci. Technol.* **1999**, *29*, 1–46. https://doi.org/10.1080/10643389991259164.
8. Monga, A.; Fulke, A.B.; Dasgupta, D. Recent developments in essentiality of trivalent chromium and toxicity of hexavalent chromium: Implications on human health and remediation strategies. *J. Hazard. Mater. Adv.* **2022**, *7*, 100113. https://doi.org/10.1016/j.hazadv.2022.100113.
9. Fulke, A.B.; Ratanpal, S.; Sonker, S. Understanding heavy metal toxicity: Implications on human health, marine ecosystems and bioremediation strategies. *Mar. Pollut. Bull.* **2024**, *206*, 116707. https://doi.org/10.1016/j.marpolbul.2024.116707.
10. Fu, S.-C.; Liu, J.-M.; Lee, K.-I.; Tang, F.-C.; Fang, K.-M.; Yang, C.-Y.; Su, C.-C.; Chen, H.-H.; Hsu, R.-J.; Chen, Y.-W. Cr(VI) induces ROS-mediated mitochondrial-dependent apoptosis in neuronal cells via the activation of Akt/ERK/AMPK signaling pathway. *Toxicol. Vitr.* **2020**, *65*, 104795. https://doi.org/10.1016/j.tiv.2020.104795.
11. Karthik, R.; Meenakshi, S. Removal of hexavalent chromium ions using polyaniline/silica gel composite. *J. Water Process Eng.* **2014**, *1*, 37–45. https://doi.org/10.1016/j.jwpe.2014.03.001.
12. World Health Organization. *Guidelines for Drinking-Water Quality*, 3rd ed.; World Health Organization: Geneva, Switzerland, 2006.
13. McKay, G.; Bino, M.J.; Altamemi, A.R. The adsorption of various pollutants from aqueous solutions on to activated carbon. *Water Res.* **1985**, *19*, 491–495. https://doi.org/10.1016/0043-1354(85)90041-7.
14. Xanthopoulou, M.; Katsoyiannis, I.A. Enhanced Adsorption of Chromate and Arsenate Ions from Contaminated Water with Emphasis on Polyethylenimine Modified Materials: A Review. *Separations* **2023**, *10*, 441. https://doi.org/10.3390/separations10080441.
15. Babel, S.; Kurniawan, T.A. Cr(VI) removal from synthetic wastewater using coconut shell charcoal and commercial activated carbon modified with oxidizing agents and/or chitosan. *Chemosphere* **2004**, *54*, 951–967. https://doi.org/10.1016/j.chemosphere.2003.10.001.

16. Gürsel, S.; Recepoğlu, Y.K.; Arar, Ö.; Arda, M. Ba^{2+} Removal from Water Using Sulfonated Polymer-Based Enhanced Ultrafiltration: Insights Into Process Optimization and Mechanism. *Int. J. Polym. Sci.* **2026**, *2026*, 8891077. https://doi.org/10.1155/ijps/8891077.
17. Urquijo, C.; Maldonado, M. Surface Modification of Poly(butyl methacrylate) with Sulfomethylated Resorcinarenes for the Selective Extraction of Dichromate Ion in Aqueous Media. *Analytica* **2025**, *6*, 24. https://doi.org/10.3390/analytica6030024.
18. Huang, L.; Jiao, X.; Lin, J.; Hao, J.; Tan, L.; Zeng, D.; Wang, S.; Lu, Y.; Shen, X.; Zhang, Z.; et al. EGDE-induced crosslinking of PEI@D500 adsorbents for direct air capture: Enhanced hydrothermal and oxidative stability. *Chem. Eng. J.* **2026**, *537*, 176243. https://doi.org/10.1016/j.cej.2026.176243.
19. Chandra, A.; Singh, A.A.; Prasad, S.; Andersson, M.R.; Gedefaw, D. Crosslinking Approaches for Polyethylene Imine (PEI) and Its Uses in Adsorption of Heavy Metals, Dyes, and Carbon Dioxide. *Appl. Sci.* **2025**, *15*, 4767. https://doi.org/10.3390/app15094767.
20. Mudau, F.H.; Mahlangu, O.T.; Makwakwa, D.H.; De Kock, L.-A.; Motsa, M.M. Post-treatment effects on polyethyleneimine/poly(sodium styrene sulfonate)-silver modified ultrafiltration membranes for slaughterhouse wastewater reuse. *J. Environ. Chem. Eng.* **2025**, *13*, 119638. https://doi.org/10.1016/j.jece.2025.119638.
21. Ayalew, Z.M.; Guo, X.; Zhang, X. Synthesis and application of polyethyleneimine (PEI)-based composite/nanocomposite material for heavy metals removal from wastewater: A critical review. *JHM Adv.* **2022**, *8*, 100158. https://doi.org/10.1016/j.hazadv.2022.100158.
22. Larsson, M.; Nosrati, A.; Kaur, S.; Wagner, J.; Baus, U.; Nydén, M. Copper removal from acid mine drainage-polluted water using glutaraldehyde-polyethyleneimine modified diatomaceous earth particles. *Heliyon* **2018**, *4*, e00520. https://doi.org/10.1016/j.heliyon.2018.e00520.
23. Lindén, J.B.; Larsson, M.; Coad, B.R.; Skinner, W.M.; Nydén, M. Polyethyleneimine for copper absorption: Kinetics, selectivity and efficiency in artificial seawater. *RSC Adv.* **2014**, *4*, 25063–25066. https://doi.org/10.1039/C4RA02223H.
24. Swamy, A.Y.; Prasad, S.; Pan, X.; Andersson, M.R.; Gedefaw, D. Glutaraldehyde and Glyoxal Crosslinked Polyethylenimine for Copper Ion Adsorption from Water. *ChemistrySelect* **2022**, *7*, e202104318. https://doi.org/10.1002/slct.202104318.
25. Elmas, S.; Gedefaw, D.A.; Larsson, M.; Ying, Y.; Cavallaro, A.; Andersson, G.G.; Nydén, M.; Andersson, M.R. Porous PEI Coating for Copper Ion Storage and Its Controlled Electrochemical Release. *Adv. Sustain. Syst.* **2020**, *4*, 1900123. https://doi.org/10.1002/adsu.201900123.
26. Liu, W.; Wang, M.; Wen, Z.; Li, Z.; Yang, L.; Jiang, C. Recyclable functionalized polymer films for the efficient removal of hexavalent chromium from aqueous solutions. *RSC Adv.* **2019**, *9*, 36751–36757. https://doi.org/10.1039/C9RA06595D.
27. Duhan, M.; Kaur, R. Nano-Structured Polyaniline as a Potential Adsorbent for Methylene Blue Dye Removal from Effluent. *J. Compos. Sci.* **2021**, *5*, 7. https://doi.org/10.3390/jcs5010007.
28. Beygisangchin, M.; Abdul Rashid, S.; Shafie, S.; Sadrolhosseini, A.R.; Lim, H.N. Preparations, Properties, and Applications of Polyaniline and Polyaniline Thin Films—A Review. *Polymers* **2021**, *13*, 2003. https://doi.org/10.3390/polym13122003.
29. Samadi, A.; Xie, M.; Li, J.; Shon, H.; Zheng, C.; Zhao, S. Polyaniline-based adsorbents for aqueous pollutants removal: A review. *Chem. Eng. J.* **2021**, *418*, 129425. https://doi.org/10.1016/j.cej.2021.129425.
30. Ali, V.; Kaur, R.; Kamal, N.; Singh, S.; Jain, S.C.; Kang, H.P.S.; Zulfequar, M.; Husain, M. Use of Cu+1 dopant and it's doping effects on polyaniline conducting system in water and tetrahydrofuran. *J. Phys. Chem. Solids* **2006**, *67*, 659–664. https://doi.org/10.1016/j.jpcs.2005.10.172.
31. Abu-Thabit, N.Y. Chemical Oxidative Polymerization of Polyaniline: A Practical Approach for Preparation of Smart Conductive Textiles. *J. Chem. Educ.* **2016**, *93*, 1606–1611. https://doi.org/10.1021/acs.jchemed.6b00060.
32. Majeed, A.H.; Mohammed, L.A.; Hammoodi, O.G.; Sehgal, S.; Alheety, M.A.; Saxena, K.K.; Dadoosh, S.A.; Mohammed, I.K.; Jasim, M.M.; Salmaan, N.U. A Review on Polyaniline: Synthesis, Properties, Nanocomposites, and Electrochemical Applications. *Int. J. Polym. Sci.* **2022**, *2022*, 9047554. https://doi.org/10.1155/2022/9047554.
33. Eskandari, E.; Kosari, M.; Davood Abadi Farahani, M.H.; Khiavi, N.D.; Saeedikhani, M.; Katal, R.; Zarinejad, M. A review on polyaniline-based materials applications in heavy metals removal and catalytic processes. *Sep. Purif. Technol.* **2020**, *231*, 115901. https://doi.org/10.1016/j.seppur.2019.115901.
34. Harijan, D.K.L.; Chandra, V. Magnetite/graphene/polyaniline composite for removal of aqueous hexavalent chromium. *J. Appl. Polym. Sci.* **2016**, *133*, 44002. https://doi.org/10.1002/app.44002.
35. Bhaumik, M.; Maity, A.; Brink, H.G. Highly efficient removal of Pb^{2+} from aqueous solution using polyaniline-cobalt composite nanorods: Kinetics, isotherm and mechanistic investigation. *Chemosphere* **2025**, *370*, 143929. https://doi.org/10.1016/j.chemosphere.2024.143929.

36. FEI Inspect F50 Field Emission SEM. Available online: https://researchnow.flinders.edu.au/en/equipments/fei-inspect-f50-field-emission-sem/ (accessed on 22 October 2026).
37. Lace, A.; Ryan, D.; Bowkett, M.; Cleary, J. Chromium Monitoring in Water by Colorimetry Using Optimised 1,5-Diphenylcarbazide Method. *Int. J. Environ. Res. Public Health* **2019**, *16*, 1803. https://doi.org/10.3390/ijerph16101803.
38. Bouzid, H.; Prosa, M.; Bolognesi, M.; Chehata, N.; Gedefaw, D.; Albonetti, C.; Andersson, M.R.; Muccini, M.; Bouazizi, A.; Seri, M. Impact of environmentally friendly processing solvents on the properties of blade-coated polymer solar cells. *J. Polym. Sci. Part A Polym. Chem.* **2019**, *57*, 487–494. https://doi.org/10.1002/pola.29286.
39. Aynaou, A.; Youbi, B.; Ait Himi, M.; Lghazi, Y.; Bahar, J.; El Haimer, C.; Ouedrhiri, A.; Bimaghra, I. Electropolymerization investigation of polyaniline films on ITO substrate. *Mater. Today Proc.* **2022**, *66*, 335–340. https://doi.org/10.1016/j.matpr.2022.05.437.
40. Kaitsuka, Y.; Hayashi, N.; Shimokawa, T.; Togawa, E.; Goto, H. Synthesis of Polyaniline (PANI) in Nano-Reaction Field of Cellulose Nanofiber (CNF), and Carbonization. *Polymers* **2016**, *8*, 40. https://doi.org/10.3390/polym8020040.
41. Ajjan, F.N.; Jafari, M.J.; Rębiś, T.; Ederth, T.; Inganäs, O. Spectroelectrochemical investigation of redox states in a polypyrrole/lignin composite electrode material. *J. Mater. Chem. A* **2015**, *3*, 12927–12937. https://doi.org/10.1039/C5TA00788G.
42. Wu, F.-C.; Tseng, R.-L.; Juang, R.-S. Characteristics of Elovich equation used for the analysis of adsorption kinetics in dye-chitosan systems. *Chem. Eng. J.* **2009**, *150*, 366–373. https://doi.org/10.1016/j.cej.2009.01.014.
43. Largitte, L.; Pasquier, R. A review of the kinetics adsorption models and their application to the adsorption of lead by an activated carbon. *Chem. Eng. Res. Des.* **2016**, *109*, 495–504. https://doi.org/10.1016/j.cherd.2016.02.006.
44. Edet, U.A.; Ifelebuegu, A.O. Kinetics, Isotherms, and Thermodynamic Modeling of the Adsorption of Phosphates from Model Wastewater Using Recycled Brick Waste. *Processes* **2020**, *8*, 665. https://doi.org/10.3390/pr8060665.
45. Yuan, X.; Xia, W.; An, J.; Yin, J.; Zhou, X.; Yang, W. Kinetic and Thermodynamic Studies on the Phosphate Adsorption Removal by Dolomite Mineral. *J. Chem.* **2015**, *2015*, 853105. https://doi.org/10.1155/2015/853105.
46. Tran, H.N. Applying Linear Forms of Pseudo-Second-Order Kinetic Model for Feasibly Identifying Errors in the Initial Periods of Time-Dependent Adsorption Datasets. *Water* **2023**, *15*, 1231. https://doi.org/10.3390/w15061231.
47. Zhang, R.; Ma, H.; Wang, B. Removal of Chromium(VI) from Aqueous Solutions Using Polyaniline Doped with Sulfuric Acid. *Ind. Eng. Chem. Res.* **2010**, *49*, 9998–10004. https://doi.org/10.1021/ie1008794.
48. Saad, D.M.G.; Cukrowska, E.M.; Tutu, H. Sulfonated cross-linked polyethylenimine for selective removal of mercury from aqueous solutions. *Environ. Toxicol. Chem.* **2012**, *94*, 1916–1929. https://doi.org/10.1080/02772248.2012.736997.
49. Kostoglou, M.; Karapantsios, T.D. Why Is the Linearized Form of Pseudo-Second Order Adsorption Kinetic Model So Successful in Fitting Batch Adsorption Experimental Data? *Colloids Interfaces* **2022**, *6*, 55. https://doi.org/10.3390/colloids6040055.
50. Boparai, H.K.; Joseph, M.; O'Carroll, D.M. Kinetics and thermodynamics of cadmium ion removal by adsorption onto nano zerovalent iron particles. *J. Hazard. Mater.* **2011**, *186*, 458–465. https://doi.org/10.1016/j.jhazmat.2010.11.029.
51. Mustapha, S.; Shuaib, D.T.; Ndamitso, M.M.; Etsuyankpa, M.B.; Sumaila, A.; Mohammed, U.M.; Nasirudeen, M.B. Adsorption isotherm, kinetic and thermodynamic studies for the removal of Pb(II), Cd(II), Zn(II) and Cu(II) ions from aqueous solutions using Albizia lebbeck pods. *Appl. Water Sci.* **2019**, *9*, 142. https://doi.org/10.1007/s13201-019-1021-x.
52. Kalam, S.; Abu-Khamsin, S.A.; Kamal, M.S.; Patil, S. Surfactant Adsorption Isotherms: A Review. *ACS Omega* **2021**, *6*, 32342–32348. https://doi.org/10.1021/acsomega.1c04661.
53. Huang, Y.-T.; Shih, M.-C. Kinetic, Isotherm, and Thermodynamic Modeling of Methylene Blue Adsorption Using Natural Rice Husk: A Sustainable Approach. *Separations* **2025**, *12*, 189.
54. Benmessaoud, A.; Nibou, D.; Mekatel, E.H.; Amokrane, S. A Comparative Study of the Linear and Non-Linear Methods for Determination of the Optimum Equilibrium Isotherm for Adsorption of Pb^{2+} Ions onto Algerian Treated Clay. *Iran. J. Chem. Chem. Eng.* **2020**, *39*, 153–171. https://doi.org/10.30492/ijcce.2019.35116.
55. Guo, M.; Guo, H.; Liu, S.; Sun, Y.; Guo, X. A microporous cationic metal–organic framework for the efficient removal of dichromate and the selective adsorption of dyes from water. *RSC Adv.* **2017**, *7*, 51021–51026. https://doi.org/10.1039/c7ra09429a.
56. Shen, Y.; Duan, R.; Qian, J.; Li, Q. Preparation of Highly Stable DUT-52 Materials and Adsorption of Dichromate Ions in Aqueous Solution. *ACS Omega* **2022**, *7*, 16414–16421. https://doi.org/10.1021/acsomega.2c00373.
57. Madri, R.K.; Tiwari, D.; Sinha, I. Efficient removal of chromate ions from aqueous solution using a highly cost-effective ferric coordinated [3-(2-aminoethylamino)propyl]trimethoxysilane–MCM-41 adsorbent. *RSC Adv.* **2021**, *11*, 11204–11214. https://doi.org/10.1039/d0ra07425j.

58. Shaibu, S.E.; Essien, N.S.; Anweting, I.B.; Udo, I.E.; Archibong, E.S.; Ibuotenang, N.D.; Inam, E.J.; Fapojuwo, D.P.; Akpan, N.A.; Offiong, N.-A.O. Manihot esculenta Leaves Extract Mediated Silver–Clay Nanocomposite for the Adsorption of Cadmium(II) and Chromium(VI) Ions from Aqueous Media. *Physchem* **2026**, *6*, 50. https://doi.org/10.3390/physchem6030050.
59. Varshney, G.; Yadav, S.; Duhan, M.; Tiwari, D.; Kaur, R. Polyaniline Nanofibers as a Sustainable Adsorbent for Cr(VI) and Hg(II) Ions Detoxification. *ChemistrySelect* **2026**, *11*, e03770. https://doi.org/10.1002/slct.202503770.
60. Pan, L.; Liu, Z.; Hernandez, M.V.; Schroeder, B.C.; Sun, Y.; Faul, C.F.J. Polyaniline-Based Cationic Porous Organic Polymers for Fast and Efficient Anion-Exchange-Driven Capture of $Cr_2O_7^{2-}$. *ACS Appl. Polym. Mater.* **2024**, *6*, 6416–6424. https://doi.org/10.1021/acsapm.4c00658.
61. Kubilay, S.; Demirci, S.; Can, M.; Aktas, N.; Sahiner, N. Dichromate and arsenate anion removal by PEI microgel, cryogel, and bulkgel. *J. Environ. Chem. Eng.* **2021**, *9*, 104799. https://doi.org/10.1016/j.jece.2020.104799.
62. Adam, F.; Chua, J.-H. The adsorption of palmytic acid on rice husk ash chemically modified with Al(III) ion using the sol–gel technique. *J. Colloid Interface Sci.* **2004**, *280*, 55–61. https://doi.org/10.1016/j.jcis.2004.07.006.
63. Khan, A.A.; Singh, R.P. Adsorption thermodynamics of carbofuran on Sn (IV) arsenosilicate in H^+, Na^+ and Ca^{2+} forms. *Colloids Surf.* **1987**, *24*, 33–42. https://doi.org/10.1016/0166-6622(87)80259-7.
64. Zhou, X.; Yu, X.; Maimaitiniyazi, R.; Zhang, X.; Qu, Q. Discussion on the thermodynamic calculation and adsorption spontaneity re Ofudje et al. (2023). *Heliyon* **2024**, *10*, e28188. https://doi.org/10.1016/j.heliyon.2024.e28188.
65. Maimaitiniyazi, R.; Zhou, X. Comment on the calculation of equilibrium constant and thermodynamic parameters by the distribution coefficient in Environmental Research 203 (2022) 111814. *Environ. Res.* **2022**, *210*, 112958. https://doi.org/10.1016/j.envres.2022.112958.
66. Das, S.; Samanta, A.; Gangopadhyay, G.; Jana, S. Clay-Based Nanocomposites as Recyclable Adsorbent toward Hg(II) Capture: Experimental and Theoretical Understanding. *ACS Omega* **2018**, *3*, 6283–6292. https://doi.org/10.1021/acsomega.8b00789.
67. San José, M.J.; López, R.; Alvarez, S.; Peñas, F.J. Bioadsorbents for the Removal of Pollutants in Wastewater: Adsorption Kinetics, Validation Test Using Methylene Blue and Methyl Orange. *Appl. Sci.* **2026**, *16*, 1512.
68. Jiang, Y.; Liu, Z.; Zeng, G.; Liu, Y.; Shao, B.; Li, Z.; Liu, Y.; Zhang, W.; He, Q. Polyaniline-based adsorbents for removal of hexavalent chromium from aqueous solution: A mini review. *Environ. Sci. Pollut. Res.* **2018**, *25*, 6158–6174. https://doi.org/10.1007/s11356-017-1188-3.
69. Golba, S.; Popczyk, M.; Miga, S.; Jurek-Suliga, J.; Zubko, M.; Kubisztal, J.; Balin, K. Impact of Acidity Profile on Nascent Polyaniline in the Modified Rapid Mixing Process—Material Electrical Conductivity and Morphological Study. *Materials* **2020**, *13*, 5108. https://doi.org/10.3390/ma13225108.
70. Ćirić-Marjanović, G.; Dragičević, L.; Milojević, M.; Mojović, M.; Mentus, S.; Dojčinović, B.; Marjanović, B.; Stejskal, J. Synthesis and Characterization of Self-Assembled Polyaniline Nanotubes/Silica Nanocomposites. *J. Phys. Chem. B* **2009**, *113*, 7116–7127. https://doi.org/10.1021/jp900096b.
71. Ćirić-Marjanović, G.; Dondur, V.; Milojević, M.; Mojović, M.; Mentus, S.; Radulović, A.; Vuković, Z.; Stejskal, J. Synthesis and Characterization of Conducting Self-Assembled Polyaniline Nanotubes/Zeolite Nanocomposite. *Langmuir* **2009**, *25*, 3122–3131. https://doi.org/10.1021/la8030396.
72. Tangtubtim, S.; Saikrasun, S. Adsorption behavior of polyethyleneimine-carbamate linked pineapple leaf fiber for Cr(VI) removal. *Appl. Surf. Sci.* **2019**, *467–468*, 596–607. https://doi.org/10.1016/j.apsusc.2018.10.204.

Disclaimer/Publisher's Note: The statements, opinions and data contained in all publications are solely those of the individual author(s) and contributor(s) and not of MDPI and/or the editor(s). MDPI and/or the editor(s) disclaim responsibility for any injury to people or property resulting from any ideas, methods, instructions or products referred to in the content.